

1 **Reaction of SO₃ with H₂SO₄ and Its Implication for Aerosol**
2 **Particle Formation in the Gas Phase and at the Air-Water**
3 **Interface**

4 **Rui Wang^a, Yang Cheng^{a,‡}, Shasha Chen^{a,‡}, Rongrong Li^a, Yue Hu^a, Xiaokai Guo^c,**
5 **Tianlei Zhang^{a,*}, Fengmin Song^a, Hao Li^{b,*}**

6 ^a *Shaanxi Key Laboratory of Catalysis, School of Chemical & Environment Science, Shaanxi*
7 *University of Technology, Hanzhong, Shaanxi 723001, P. R. China*

8 ^b *State Key Joint Laboratory of Environment Simulation and Pollution Control, Research Center*
9 *for Eco-environmental Sciences, Chinese Academy of Sciences, Beijing, 100085, China*

10 ^c *Department of Applied Chemistry, Yuncheng University, Yuncheng, Shanxi 044000, China*

11 **Abstract**

12 The reactions between SO₃ and atmospheric acids are indispensable in improving the formation of
13 aerosol particle. However, relative to those of SO₃ with organic acids, the reaction of SO₃ with
14 inorganic acids has not received much attention. Here, we explore the atmospheric reaction between
15 SO₃ and H₂SO₄, a typical inorganic acid, in the gas phase and at the air-water interface by using
16 quantum chemical (QC) calculations and Born-Oppenheimer molecular dynamics simulations. We
17 also report the effect of H₂S₂O₇, the product of the reaction between SO₃ and H₂SO₄, on new particle
18 formation (NPF) in various environments by using the Atmospheric Cluster Dynamics Code kinetic
19 model and the QC calculation. The present findings show that the gas phase reactions of SO₃ +
20 H₂SO₄ without and with water molecule are both low energy barrier processes. With the
21 involvement of interfacial water molecules, H₂O-induced the formation of S₂O₇²⁻⋯H₃O⁺ ion pair,
22 HSO₄⁻ mediated the formation of HSO₄⁻⋯H₃O⁺ ion pair and the deprotonation of H₂S₂O₇ were
23 observed and proceeded on the picosecond time-scale. The present findings suggest the potential
24 contribution of SO₃-H₂SO₄ reaction to NPF and aerosol particle growth as the facts that *i*) H₂S₂O₇
25 can directly participate in H₂SO₄-NH₃-based cluster formation and can present a more obvious
26 enhancement effect on SA-A-based cluster formation; and *ii*) the formed interfacial S₂O₇²⁻ can
27 attract candidate species from the gas phase to the water surface, and thus, accelerate particle growth.

* Corresponding authors. Tel: +86-0916-2641083, Fax: +86-0916-2641083.

E-mail: ztianlei88@163.com (T. L Zhang) ; haol@rcees.ac.cn (H. Li)

‡ Yang Cheng and Shasha Chen contributed equally to this work.

1. Introduction

Sulfur trioxide (SO_3) is a major air pollutant (Zhuang and Pavlish, 2012; Chen and Bhattacharya, 2013; Cao et al., 2010; Kikuchi, 2001; Mitsui et al., 2011) and can be considered as the most important oxidation product of SO_2 (Starik et al., 2004). As an active atmospheric species, SO_3 can lead to the formations of acid rain and atmospheric aerosol (Sipilä et al., 2010; Mackenzie et al., 2015; England et al., 2000; Li et al., 2016; Renard et al., 2004) and thus plays a well-documented role in regional climate and human health (Zhang et al., 2012; Pöschl, 2005; Zhang et al., 2015; Pöschl and Shiraiwa, 2015; Haywood and Boucher, 2000; Lohmann and Feichter, 2005). In the atmosphere, the hydrolysis of SO_3 to product H_2SO_4 (SA) is the most major loss route of SO_3 (Morokuma and Muguruma, 1994; Akhmatskaya et al., 1997; Larson et al., 2000; Hazra and Sinha, 2011; Long et al., 2013a; Torrent-Sucarrat et al., 2012; Ma et al., 2020). As a complement to the loss of SO_3 , ammonolysis reaction of SO_3 in polluted areas of NH_3 can form $\text{H}_2\text{NSO}_3\text{H}$, which not only can be competitive with the formation of SA from the hydrolysis reaction of SO_3 , but also can enhance the formation rates of sulfuric acid (SA)-dimethylamine ($\text{NH}(\text{CH}_3)_2$, DMA) clusters by about 2 times. Similarly, the reactions of SO_3 with CH_3OH and organic acids (such as HCOOH) were reported (Liu et al., 2019; Hazra and Sinha, 2011; Long et al., 2012; Mackenzie et al., 2015; Huff et al., 2017; Smith et al., 2017; Li et al., 2018a), and both processes can provide a mechanism for incorporating organic matter into aerosol particles. However, the reaction mechanism between SO_3 and inorganic species are still unclear.

As a major inorganic acidic air pollutant (Tilgner et al., 2021), SA can act as an important role in the new particle formation (Weber et al., 1995; Weber et al., 1996; Weber et al., 2001; Sihto et al., 2006; Riipinen et al., 2007; Sipilä et al., 2010; Zhang et al., 2012) and acid rain (Calvert et al., 1985; Finlayson-Pitts and Pitts Jr, 1986; Wayne, 2000). The source of gas-phase SA is mainly produced by the gas-phase hydrolysis reaction of SO_3 . For the direct reaction between SO_3 and H_2O , it takes place hardly in the atmosphere due to high energy barrier (Chen and Plummer, 1985; Hofmann and Schleyer, 1994; Morokuma and Muguruma, 1994; Steudel, 1995). However the addition of a second water molecule (Morokuma and Muguruma, 1994; Larson et al., 2000; Loerting and Liedl, 2000), the hydroperoxyl radical (Gonzalez et al., 2010), formic acid (Hazra and Sinha, 2011; Long et al., 2012), sulfuric acid (Torrent-Sucarrat et al., 2012), nitric acid (Long et al., 2013a),

1 oxalic acid (Lv et al., 2019) and ammonia (Bandyopadhyay et al., 2017) have been reported to
2 catalyze the formation of SA from the hydrolysis reaction of SO_3 as they can promote atmospheric
3 proton transfer reactions. Similarly, as SA can give out protons more readily than H_2O , which in
4 turn is more conducive to the proton transfer, thus we predict that the addition reaction involving
5 the proton transfer between SO_3 and SA is much easier under atmospheric conditions than that
6 between SO_3 and H_2O . However, this gas-phase reaction has not been investigated as far as we
7 know. Previous studies have shown that the concentration of water vapor decreases significantly
8 with increasing altitude (Anglada et al., 2013), leading to longer atmospheric lifetimes of SO_3 . The
9 gas phase reaction of SO_3 with H_2SO_4 may contribute significantly to the loss of SO_3 in dry areas
10 where $[\text{H}_2\text{SO}_4]$ is relatively high (especially at lower temperatures) and at higher altitude. So, it is
11 important to study the reaction mechanism of SO_3 with H_2SO_4 and its competition with H_2O -assisted
12 hydrolysis of SO_3 . Meanwhile, in many gas phase reactions, single water molecule can play a
13 catalyst role by increasing the stability of pre-reactive complexes and reducing the activation energy
14 of transition states (Kanno et al., 2006; Stone and Rowley, 2005; Chen et al., 2014; Viegas and
15 Varandas, 2012, 2016). For example, single water molecule in the $\text{H}_2\text{O}\cdots\text{HO}_2 + \text{SO}_3$ reaction can
16 catalyze the formation of HSO_5 (Gonzalez et al., 2010). Thus, it is equally important to study the
17 $\text{SO}_3 + \text{SA}$ reaction without and with H_2O . In addition to the gas phase reactions, many new
18 atmospheric processes and new reaction pathways have been observed at the air-water interface
19 (Zhong et al., 2017; Kumar et al., 2017; Kumar et al., 2018; Zhu et al., 2016; Li et al., 2016; Zhu et
20 al., 2017). Such as, the organic acids reacting with SO_3 can form the ion pair of carboxylic sulfuric
21 anhydride and hydronium at the air-water interface (Zhong et al., 2019). This mechanism is different
22 from the gas phase reaction in which the organic acid either serves as a catalyst for the hydrolysis
23 of SO_3 or acts as a reactant reacting with SO_3 directly. So, water droplets may play important roles
24 in atmospheric behaviors between SO_3 and SA. Thus, it is also important to study the interfacial
25 mechanism between SO_3 and SA, and to compare its difference with the corresponding gas-phase
26 reaction.

27 Previous experimental studies (Otto and Steudel, 2001; Abedi and Farrokhpour, 2013) found
28 that disulfuric acid ($\text{H}_2\text{S}_2\text{O}_7$, DSA) is the product of the reaction between SO_3 and SA. From the
29 perspective of structure, DSA possesses two HO functional groups. Both HO groups can act as
30 hydrogen donors and acceptors to interact with atmospheric particle precursors. It has been shown

1 that the reaction between SO_3 and some important atmospheric species (Li et al., 2018a; Yang et al.,
2 2021; Liu et al., 2019; Rong et al., 2020) not only can cause appreciable consumption of SO_3 and
3 thus reduce the abundance of SA from the hydrolysis of SO_3 in the atmosphere, but also can promote
4 NPF process by their products. For example, the products of $\text{NH}_2\text{SO}_3\text{H}$, $\text{HOOCOOSO}_3\text{H}$,
5 $\text{CH}_3\text{OSO}_3\text{H}$ and $\text{HOCCOOSO}_3\text{H}$ from the reactions of SO_3 with NH_3 (Li et al., 2018a), $\text{H}_2\text{C}_2\text{O}_4$
6 (Yang et al., 2021), CH_3OH (Liu et al., 2019) and HOOCCHO (Rong et al., 2020) all have a catalytic
7 effect on the formation of new particles in aerosols. However, whether DSA produced by the
8 reaction between SO_3 and SA contributes to aerosol formation or not is still unclear. Thus, another
9 main question that we intend to address here is the role of DSA in atmospheric SA- NH_3 (A)
10 nucleation, which have been recognized as dominant precursors in highly polluted areas, especially
11 in some megacities in Asia.

12 In this work, using quantum chemical calculations and Master Equation, we first studied the
13 gas-phase reaction between SO_3 and SA to product DSA with H_2O acting as a catalyst. Then, we
14 use the Born-Oppenheimer Molecular Dynamic (BOMD) simulations to evaluate the reaction
15 mechanism of SO_3 with SA at the air-water interface. Finally, we used Atmospheric Clusters
16 Dynamic Code (ACDC) and quantum chemical calculations to investigate atmospheric
17 implications of SO_3 -SA reaction to the atmospheric particle formation. Particular attention of this
18 work is focused on the study of *i*) the mechanism difference of the $\text{SO}_3 + \text{SA}$ reaction in the gas
19 phase and at the air-water interface; *ii*) the fate of DSA in atmospheric NPF and its influence at
20 various environmental conditions.

21 **2. Computational Details**

22 **2.1 Quantum Chemical Calculation.** The M06-2X functional has been proved to be one
23 of the best functionals to describe the noncovalent interactions and estimate the
24 thermochemistry and equilibrium structures for atmospheric reactions (Elm et al., 2012;
25 Mardirossian and Head-Gordon, 2016). So, for the $\text{SO}_3 + \text{SA}$ reaction without and with water
26 molecule in the gas phase, the optimized geometries and vibrational frequencies of reactants,
27 pre-reactive complexes, transition states (TSSs), post-reactive complexes and products were
28 calculated using M06-2X method (Zhao and Truhlar, 2008; Elm et al., 2012) with 6-
29 311++G(2df,2pd) basis set by Gaussian 09 packages (Frisch, 2009). It is noted that the calculated

1 bond distances and bond angles at the M06-2X/6-311++G(3df,2pd) level (Fig. S1) agree well with
2 the available experimental values (Kuczkowski et al., 1981). At the same level, the connectivity
3 between the TSs and the suitable pre- and post-reactant complexes was performed by intrinsic
4 reaction coordinate (IRC) calculations. Then, single point energy calculations were calculated at the
5 CCSD(T)-F12/cc-pVDZ-F12 level (Adler et al., 2007; Knizia et al., 2009) by using ORCA (Neese,
6 2012).

7 A multistep global minimum sampling technique was used to search for the global minima of
8 the (DSA)_x(SA)_y(A)_z ($z \leq x + y \leq 3$) molecular clusters. Specifically, a multistep global minimum
9 sampling technique was used to search for the global minima of the (SA)_x(A)_y(DSA)_z ($0 < y \leq x +$
10 $z \leq 3$) clusters. Specifically, the initial $n \times 1000$ ($1 < n < 5$) configurations for each cluster were
11 systematically generated by the ABCcluster program (Zhang and Dolg, 2015), and were optimized
12 at the semi-empirical PM6 (Stewart, 2013) methods using MOPAC 2016 (Stewart, 2013; Stewart,
13 2007). Then, up to $n \times 100$ structures with relatively lowest energy among the $n \times 1000$ ($1 < n < 5$)
14 structures were selected and reoptimized at the M06-2X/6-31+G(d,p) level. Finally, $n \times 10$ lowest-
15 lying structures were optimized by the M06-2X/6-311++G(2df,2pd) level to determine the global
16 minimum. To obtain the reliable energies, single-point energy calculations were refined at the
17 DLPNO-CCSD(T)/aug-cc-pVTZ level based on the optimized geometries at the M06-2X/6-
18 311++G(2df,2pd) level. The optimized structures and the formation Gibbs free energy of the stable
19 clusters were summarized in Fig. S9 and Table S8 of the *SI Appendix*, respectively.

20 **2.2 Rate constant calculations.** Using the Rice-Ramsperger-Kassel-Marcus based Master
21 Equation (ME/RRKM) model (Miller and Klippenstein, 2006), the kinetics for the SO₃ + SA
22 reaction without and with water molecule were calculated by adopting a Master Equation Solver
23 for Multi Energy-well Reactions (MESMER) code (Glowacki et al., 2012). In the MESMER
24 calculation, the rate coefficients for the bimolecular barrierless association step (from reactants to
25 pre-reactive complexes) were evaluated by the Inverse Laplace Transform (ILT) method (Horváth
26 et al., 2020), meanwhile the unimolecular step was performed by the RRKM theory combined with
27 the asymmetric Eckart model. The ILT method and RRKM theory can be represented in Eq (1) and
28 Eq (2), respectively.

$$k^\infty(\beta) = \frac{1}{Q(\beta)} \int_0^\infty k(E) \rho(E) \exp(-\beta E) dE \quad (1)$$

29

$$k(E) = \frac{W(E - E_0)}{h\rho(E)} \quad (2)$$

1
2
3
4
5
6
7
8
9
10
11
12
13
14
15
16
17
18
19
20
21
22
23
24
25
26
27
28
29

Where h is denoted as Planck's constant; $\rho(E)$ is denoted as the active density of state of the reactant at energy level E ; E_0 is denoted as the reaction threshold energy and $W(E-E_0)$ is denoted as the sum of the rovibrational states of the transition state (TS) geometry (excluding the degree of freedom related to passing the transition state). The input parameters for electronic geometries, vibrational frequencies, and rotational constants were calculated at the M06-2X/6-311++G(2df,2pd) level and single-point energy calculations were refined at the CCSD(T)-F12/cc-pVDZ-F12 level for the modeling.

2.3 Born-Oppenheimer Molecular Dynamic (BOMD) Simulation. The CP2K code (Hutter et al., 2014) was used in the BOMD simulations. The Becke-Lee-Yang-Parr (BLYP) functional (Becke, 1988; Lee et al., 1988) was chosen to treat with the exchange and correlation interactions, and the Grimme's dispersion was carried out to account for the weak dispersion interaction (Grimme et al., 2010). The Goedecker-Teter-Hutter (GTH) conservation pseudopotential (Goedecker et al., 1996; Hartwigsen et al., 1998) with the Gaussian DZVP basis set (VandeVondele and Hutter, 2007) and the auxiliary plane wave basis set was applied to correct the system valence electrons and the core electrons, respectively. For the plane wave basis set and Gaussian basis set, the energy cut off (Zhong et al., 2017; Zhong et al., 2018; Zhong et al., 2019) were set to 280 and 40 Ry, respectively. For each simulation in the gas phase, a $15 \times 15 \times 15 \text{ \AA}^3$ supercell with periodic boundary condition was adopted with a time step of 0.5 fs. As the droplet system with 191 water molecules are sufficient to describe the interfacial mechanism (Zhong et al., 2017), the air-water interfacial system here included 191 water molecules, SO_3 and SA in the BOMD simulation. It is pointed out that the droplet system with 191 water molecules has been equilibrated before SO_3 and H_2SO_4 was added at the water surface. The details of the equilibrium process for the droplet system with 191 water molecules are shown in the *SI Appendix* Part 4. To avoid periodic interactions between adjacent water droplets, the size of the simulation box (Kumar et al., 2017; Kumar et al., 2018; Ma et al., 2020) was set as $35 \times 35 \times 35 \text{ \AA}^3$ with a time step of 1.0 fs. Notably, the timestep of 1.0 fs has been proved to achieve sufficient energy conservation for the water system (Zhong et al., 2015; Li et al., 2016; Zhu et al., 2016; Kumar et al., 2017). For all the simulations in the gas phase and at

1 the air-water interface, the Nose-Hoover thermostat (Zhong et al., 2017; Zhong et al., 2018;
 2 Zhong et al., 2019; Kumar et al., 2017; Kumar et al., 2018; Ma et al., 2020) was selected the
 3 NVT ensemble to control the temperature around 300 K. To eliminate the influence of the initial
 4 configuration on the simulation results of interfacial reaction, 40 BOMD simulations for the air-
 5 water interface reactions were carried out.

6 **2.4 Atmospheric Clusters Dynamic Code (ACDC) Model**

7 The Atmospheric Cluster Dynamics Code (ACDC) (McGrath et al., 2012) was used to
 8 simulate the cluster formation rates and mechanisms of (DSA)_x(SA)_y(A)_z ($z \leq x + y \leq 3$) clusters
 9 at different temperatures and monomer concentrations. The thermodynamic data of quantum
 10 chemical calculation at the DLPNO-CCSD(T)/aug-cc-pVTZ//M06-2X/6-311++G(2df,2pd)
 11 level of theory can be used as the input of ACDC. The birth-death equation (Eq. 3) for clusters
 12 solves the time development of cluster concentrations by numerical integration using the ode15s
 13 solver in MATLAB program (Shampine and Reichelt, 1997).

$$14 \quad \frac{dc_i}{dt} = \frac{1}{2} \sum_{j < i} \beta_{j,(i-j)} C_j C_{(i-j)} + \sum_j \gamma_{(i+j) \rightarrow i} C_{i+j} - \sum_j \beta_{i,j} C_i C_j - \frac{1}{2} \sum_{j < i} \gamma_{i \rightarrow j} C_i + Q_i - S_i \quad (3)$$

15 Where c_i is the concentration of cluster i ; β_{ij} is the collision coefficient between clusters i and
 16 j ; $\gamma_{(i+j) \rightarrow i}$ is the evaporation coefficient of cluster $i+j$ evaporating into clusters i and j , and Q_i is all
 17 other source term of cluster i . (See more details of β and γ in *SI Appendix* Part 4). Besides, a
 18 constant coagulation sink coefficient $2 \times 10^{-2} \text{ s}^{-1}$ (corresponding to the median observed in
 19 contaminated areas) was used for taking into account external losses (Yao et al., 2018; Zhang
 20 et al., 2022; Liu et al., 2021b). The boundary conditions in the ACDC require that the smallest
 21 clusters outside of the simulated system should be very stable so that not to evaporate back
 22 immediately (McGrath et al., 2012). Based on cluster volatilization rate (shown in Table S10) and
 23 the formation Gibbs free energy of the clusters (shown in Table S8), the cluster boundary conditions
 24 simulated in this study were set as (SA)₄·(A)₃, (SA)₄·(A)₄, SA·(A)₃·(DSA)₃, (SA)₃·(A)₄·(DSA)₁ and
 25 (SA)₂·(A)₃·(DSA)₂. According to field observations, the concentration of SA and A was respectively
 26 set in a range of 10^6 - 10^8 molecules·cm⁻³ and 10^7 - 10^{11} molecules·cm⁻³ (Almeida et al., 2013; Kuang
 27 et al., 2008; Bouo et al., 2011; Zhang et al., 2018). As the prediction in Table S7, the concentration
 28 of DSA is set to 10^4 - 10^8 molecules·cm⁻³. However, DSA is easily hydrolyzed with abundant water
 29 in the troposphere to form H₂SO₄, the concentration of DSA listed in Fig. S9 was overestimated.

1 So, the maximum concentration of DSA (10^8 molecules·cm⁻³) was not included in the effect of
2 H₂S₂O₇ on new particle formation (NPF) in various environments. Besides, the temperature was set
3 to be 218.15-298.15 K, which span most regions of the troposphere and the polluted atmospheric
4 boundary layer.

5 **3. Results and discussion**

6 **3.1 Reactions in the gas phase**

7 The addition reaction involving the proton transfer between SO₃ and SA (Channel DSA)
8 proceeded through the formation of SO₃···H₂SO₄ complex followed by unimolecular transformation
9 through transition state TS_{DSA} to form H₂S₂O₇ (Fig. 1(a)). The reactant complex SO₃···H₂SO₄ was
10 a double six-membered ring complex with a relative Gibbs free energy of -1.6 kcal·mol⁻¹. After the
11 formation of SO₃···H₂SO₄ complex, Channel DSA overcame a Gibbs free energy barrier of 2.3
12 kcal·mol⁻¹, which was lower by 4.2 kcal·mol⁻¹ than that of H₂O-catalyzed hydrolysis of SO₃ (Fig.
13 S1). Rate constant for the SO₃ + SA reaction was calculated at various temperatures (Table 1).
14 Within the temperature range of 280-320 K, the rate constants for the SO₃ + SA reaction were
15 calculated to be 2.57×10^{-12} - 5.52×10^{-12} cm³·molecule⁻¹·s⁻¹, which were larger by 3.43-4.03 times
16 than the corresponding values of H₂O-catalyzed hydrolysis of SO₃. Therefore, it can be said that the
17 direct reaction between SO₃ and SA occurs easily under atmospheric conditions.

18 The SO₃ + H₂SO₄ reaction with H₂O produced two distinct products, labeled (i) H₂S₂O₇ (DSA,
19 Channel DSA_WM) and (ii) H₂SO₄ (SA, Channel SA_SA). A single water molecule in (i) acted as
20 a catalyst, while it played as a reactant in (ii). The schematic potential energy surface for the SO₃ +
21 H₂SO₄ reaction with H₂O was shown in Fig. 1. As the probability of simultaneous collision (Pérez-
22 Ríos et al., 2014; Elm et al., 2013) of three molecules of SO₃, SA and H₂O was quite low under
23 realistic conditions, both Channel DSA_WM and Channel SA_SA can be considered as a sequential
24 bimolecular process. In other words, both Channel DSA_WM and Channel SA_SA occurred via
25 the collision between SO₃ (or H₂SO₄) and H₂O to form dimer (SO₃···H₂O and H₂SO₄···H₂O) first,
26 and then the dimer encountered with the third reactant H₂SO₄ or SO₃. The computed Gibbs free
27 energies of dimer complexes SO₃···H₂O and H₂SO₄···H₂O were respectively 0.8 kcal·mol⁻¹ and -1.9
28 kcal·mol⁻¹, which were respectively consistent with the previous values (the range from -0.2 to 0.62
29 kcal·mol⁻¹ for SO₃···H₂O complex (Bandyopadhyay et al., 2017; Long et al., 2012) and the range

1 from -1.82 to -2.63 kcal·mol⁻¹ for H₂SO₄···H₂O complex (Long et al., 2013b; Tan et al., 2018)). The
2 Gibbs free energy of H₂SO₄···H₂O was lower by 2.7 kcal·mol⁻¹ than that of SO₃···H₂O, thus leading
3 to that the equilibrium constant of the former complex was larger by 1-2 orders of magnitude than
4 that of the latter one in Table S2. Additionally, the larger equilibrium constant of H₂SO₄···H₂O
5 complex led to its higher concentration in the atmosphere. For example, when the concentrations
6 of SO₃ (Yao et al., 2020), H₂SO₄ (Liu et al., 2015) and H₂O (Anglada et al., 2013) were 10⁶, 10⁸ and
7 10¹⁷ molecules·cm⁻³, respectively, the concentrations of SO₃···H₂O and H₂SO₄···H₂O were 2.41 ×
8 10³-2.01 × 10⁴ and 5.01 × 10⁵-3.01 × 10⁸ molecules·cm⁻³ within the temperature range of 280-320
9 K (see Table S3), respectively. So, we predict that Channel DSA_WM and Channel SA_SA mainly
10 take place via the collision of H₂SO₄···H₂O with SO₃. In order to check this prediction, the effective
11 rate constants for two bimolecular reactions of H₂SO₄···H₂O + SO₃ and SO₃···H₂O + H₂SO₄ were
12 calculated, and the details were shown in *SI Appendix*, Part 3 and Table 1. As seen in Table 1, the
13 SO₃···H₂O + H₂SO₄ reaction in both Channel DSA_WM and Channel SA_SA can be neglected as
14 their effective rate constants were smaller by 16.7-48.5 and 1.02-3.05 times than the corresponding
15 values in the H₂SO₄···H₂O + SO₃ reaction within the temperature range of 280-320 K, respectively.
16 Therefore, we only considered the H₂SO₄···H₂O + SO₃ bimolecular reaction in both Channel
17 DSA_WM and Channel SA_SA.

18 As for Channel DSA_WM, the H₂SO₄···H₂O + SO₃ reaction occurred in a stepwise process as
19 displayed in Fig. 1(b), which was similar to the favorable routes in the hydrolysis of COS, HCHO
20 and CH₃CHO catalyzed by sulfuric acid (Long et al., 2013b; Li et al., 2018b; Tan et al., 2018). When
21 the H₂SO₄···H₂O complex and SO₃ served as reactants, the reaction was initiated by complex
22 IM_{DSA_WM}' where a van der Waals interaction (S2···O4, 2.75 Å) was found between the O4 atom of
23 SA moiety in H₂SO₄···H₂O and the S atom of SO₃. After complex IM_{DSA_WM}', the ring enlargement
24 from IM_{DSA_WM}' to SO₃···H₂SO₄···H₂O complex occurred through transition state TS_{DSA_WM}' with
25 a Gibbs free energy barrier of 1.2 kcal·mol⁻¹. Complex IM_{DSA_WM} was 6.1 kcal·mol⁻¹ lower in energy
26 than IM_{DSA_WM}'. In IM_{DSA_WM}, SO₃ acted as double donors of hydrogen bond to form a cage-like
27 hydrogen bonding network with H₂SO₄···H₂O. Then, starting with IM_{DSA_WM} complex, the
28 H₂SO₄···H₂O + SO₃ reaction occurred through transition state TS_{DSA_WM} with a Gibbs free barrier
29 energy of 0.5 kcal·mol⁻¹ to form a quasi-planar network complex, H₂S₂O₇···H₂O. TS_{DSA_WM} was in
30 the middle of a double proton transfer, where H₂O played as a bridge for proton transfer, along with

1 the simultaneous formation of the O4...S2 bond. In order to estimate the catalytic ability of H₂O in
 2 the SO₃ + SA reaction, the effective rate constant ($k'_{\text{DSA_WM_s}}$) of the H₂SO₄...H₂O + SO₃ reaction
 3 were compared with the rate constant (k_{DSA}) of the SO₃ + H₂SO₄ reaction. As seen in Table 1, under
 4 the experimental concentration (Anglada et al., 2013) ([H₂O] = 5.20 × 10¹⁶-2.30 × 10¹⁸
 5 molecules·cm⁻³) within the temperature range of 280-320 K, the calculated $k'_{\text{DSA_WM_s}}$ was 1.03 ×
 6 10⁻¹¹-4.60 × 10⁻¹² cm³·molecule⁻¹·s⁻¹, which was larger by 1.79-1.86 times than that of k_{DSA} . This
 7 result shows that H₂O exerts catalytic role in promoting the rate of the SO₃ + H₂SO₄ reaction.

8 Regarding Channel SA_SA, the stepwise reaction occurred firstly via the ring enlargement
 9 from six-membered ring complex IM_{SA_SA}' to a cage-like hydrogen bonding network IM_{SA_SA}, and
 10 then took place by going through a transition state, TS_{SA_SA}, to form the product complex (H₂SO₄)₂.
 11 TS_{DSA_WM} was in the middle of a double hydrogen transfer, where H₂SO₄ acted as a bridge of
 12 hydrogen atom from the H₂O to SO₃ along with O1 atom of H₂O addition to the S atom of SO₃. It
 13 was worth noting that the energy barriers of two elementary reactions involved in the stepwise route
 14 of Channel SA_SA were only 1.8 and 0.6 kcal·mol⁻¹, respectively, showing that the stepwise route
 15 of Channel SA_SA is feasible to take place from energetic point of view. To check whether Channel
 16 DSA_WM is more favorable than Channel SA_SA or not, their rate ratio listed in Eq. 4 has been
 17 calculated in Table 1. The calculated rate ratio $v_{\text{DSA_WM}}/v_{\text{SA_SA}}$ shows that Channel DSA_WM is more
 18 important than Channel SA_SA because the rate ratio $v_{\text{DSA_WM}}/v_{\text{SA_SA}}$ is 1.53-3.04 within the
 19 temperature range of 280-320 K. So, we predicted that the SO₃ + H₂SO₄ reaction with H₂O
 20 producing H₂S₂O₇ is more favorable than that forming H₂SO₄.

$$21 \frac{v_{\text{DSA_WM}}}{v_{\text{SA_SA}}} = \frac{v_{\text{DSA_WM_s}} + v_{\text{DSA_WM_o}}}{v_{\text{SA_SA_s}} + v_{\text{SA_SA_o}}} = \frac{k_{\text{DSA_WM_s}} \times K_{\text{eq}(\text{H}_2\text{SO}_4 \cdots \text{H}_2\text{O})} + k_{\text{DSA_WM_o}} \times K_{\text{eq}(\text{SO}_3 \cdots \text{H}_2\text{O})}}{k_{\text{SA_SA_s}} \times K_{\text{eq}(\text{H}_2\text{SO}_4 \cdots \text{H}_2\text{O})} + k_{\text{SA_SA_o}} \times K_{\text{eq}(\text{SO}_3 \cdots \text{H}_2\text{O})}} \quad (4)$$

22 3.2 Reactions at the Air-water interface

23 The mechanism for the SO₃ + SA reaction at the air-water interface was lacking. Notably, SO₃,
 24 SA and DSA molecules can stay at the interface for 35.8%, 30.1% and 39.2% of the time in the 150
 25 ns simulation (Fig. S2), respectively, revealing that the existence of SO₃, SA and DSA at the air-
 26 water interface cannot be negligible. So, the BOMD simulations were used to evaluate the reaction
 27 mechanism of SO₃ with SA at the aqueous interfaces. Similar with the interfacial reaction of SO₃
 28 with organic and inorganic acids (Cheng et al., 2023; Zhong et al., 2019), the reaction between SO₃

1 and SA at the aqueous interface may occur in three ways: (i) SO₃ colliding with adsorbed SA at the
 2 air-water interface; (ii) SA colliding with adsorbed SO₃ at the aqueous interface; or (iii) the SO₃-SA
 3 complex reacting at the aqueous interface. However, due to the high reactivity both of SO₃ and SA
 4 at the air-water interface, the lifetimes of SO₃ (Zhong et al., 2019) and SA (Fig. S3) (on the order
 5 of a few picoseconds) on the water droplet were extremely short and can be formed SA⁻ ion quickly.
 6 Besides, as the calculated result above, SO₃···H₂SO₄ complex can be generate DSA easily before it
 7 approaches the air-water interface. So, two possible models were mainly considered for the SO₃ +
 8 SA reaction on the water surface: (i) gaseous SO₃ colliding with SA⁻ at the air-water interface and
 9 (ii) the DSA (the gas-phase product of SO₃ and SA) dissociating on water droplet.

10 ***Gaseous SO₃ Colliding with SA⁻ at the Air-Water Interface.*** At the water droplet's surface,
 11 the interaction between SO₃ and SA⁻ included two main channels: (i) H₂O-induced formation of
 12 S₂O₇²⁻···H₃O⁺ ion pair (Fig. 2, Fig. S4 and Movie S1) and (ii) SA⁻-mediated formation of SA⁻···H₃O⁺
 13 ion pair (Fig. 3, Figs. S5-S6 and Movies S2-S3). The BOMD simulations for H₂O-induced
 14 formation of S₂O₇²⁻···H₃O⁺ ion pair was illustrated in Fig. 2, the H1 atom of SA⁻ ion can combine
 15 with a nearby interfacial water molecule at 8.18 ps by hydrogen bond ($d_{(O3-H1)} = 1.17 \text{ \AA}$) interaction,
 16 thus forming hydrated hydrogen sulfate ion (SA⁻···H₂O). Then, the H1 atom of SA⁻ ion was moved
 17 to the O3 atom of the interfacial water molecule at 8.28 ps, revealing the formation of SO₄²⁻···H₃O⁺
 18 ion pair. Additionally, SO₄²⁻ gradually approached to SO₃ molecule with the shortening of S1-O1
 19 bond. At 9.26 ps, the S1-O1 bond length was 1.84 Å, which was close to the length of S-O1 (1.65
 20 Å) bond in S₂O₇²⁻ ion (Fig. S8), revealing the formation of S₂O₇²⁻···H₃O⁺ ion pair.

21 Both direct (Fig. 3(a), Fig. S5 and Movie S2) and indirect (Fig. 3(b), Fig. S6 and Movie S3)
 22 forming mechanisms were observed in SA⁻-mediated formation of SA⁻···H₃O⁺ ion pair. The direct
 23 SA⁻-mediated formation of SA⁻···H₃O⁺ ion pair was a loop structure mechanism, which was
 24 consistent with gas phase hydrolysis of SO₃ assisted by acidic catalysts of HCOOH, HNO₃, H₂C₂O₄
 25 and SA in the previous works (Long et al., 2012; Long et al., 2013a; Torrent-Sucarrat et al., 2012;
 26 Lv et al., 2019), and the interfacial reactions of HNO₃-mediated Criegee hydration (Kumar et al.,
 27 2018) and the hydration of SO₃ via the loop-structure formation (Lv and Sun, 2020). As for the
 28 direct formation mechanism of SA⁻···H₃O⁺ ion pair seen in Fig. 3(a) and movie S2, an eight-
 29 membered loop complex, SO₃···H₂O(1)···SA⁻, was found at 1.46 ps with the formations of two
 30 hydrogen bonds ($d_{(O3-H2)} = 2.13 \text{ \AA}$; $d_{(O4-H3)} = 2.18 \text{ \AA}$) and a van der Waals interaction ($d_{(S1-O1)} =$

1 2.14 Å). Subsequently, SO₃ and interfacial H₂O(1) were close to each other. At 1.59 ps, a transition
2 state-like loop structure was observed and proton transfer from interfacial H₂O(1) to another
3 suspended H₂O(2) was found, where the bond lengths of S1-O1, O1-H1 and H1-O2 were 1.94 Å,
4 1.19 Å and 1.32 Å, respectively. At 1.70 ps, the bond lengths of S-O1 and H1-O2 were reduced to
5 1.73 Å and 1.01 Å, while the bond length of H1-O2 was extended to 1.61 Å, showing the formation
6 of SA⁻···H₃O⁺ ion pair. During the direct formation route of SA⁻···H₃O⁺ ion pair, SA⁻ played as a
7 spectator, while interfacial water molecules acted as both a reactant and a proton acceptor. As
8 compared with the hydration reaction mechanism of SO₃ at the air-water interface reported by Lv
9 et al. (Lv and Sun, 2020), the loop-structure formation with proton transferred in the loop was not
10 observed in the direct mechanism of SA⁻-mediated formation of SA⁻···H₃O⁺ ion pair. This was
11 probably because SA⁻ ion was more difficult to give the proton.

12 As seen in Fig. 3(b) and Movie S3, the indirect forming process of SA⁻···H₃O⁺ ion pair
13 contained two steps: (i) SO₃ hydration along with SA formation and (ii) SA deprotonation.
14 Specifically, as for step (i), at 0.70 ps, a transition state like structure of SO₃ hydration was observed
15 with SO₃, SA⁻ and an interfacial water molecule involved. Note that at this time the H1 atom in
16 interfacial H₂O molecule migrated to the O2 atom of SA⁻ ion instead of the surrounding water
17 molecule. At 0.96 ps, the O1-H1 bond of H₂O was broken with the length of 1.56 Å, while the S1-
18 O1 bond was formed with the length of 1.75 Å, demonstrating the completion of hydrolysis reaction
19 of SO₃ and the formation of SA molecule. Then, at 8.08 ps, the H2 proton transferred from SA to
20 the O4 atom of SA⁻ ion and to the O5 atom of the nearby water molecule was occurred, where the
21 O3-H2 and O1-H3 bonds extended to 1.13 Å and 1.22 Å, and the length of O4-H2 and O5-H3 bonds
22 shortened to 1.45 Å and 1.20 Å. Finally, SA deprotonation was completed at 8.23 ps with the
23 formation of SA⁻···H₃O⁺ ion pair. During the whole indirect forming process of SA⁻···H₃O⁺ ion pair,
24 SA⁻ played as protons donor and acceptor, and water molecules acted as hydration reactants and
25 proton acceptors. Compared with the direct mechanism of SA⁻···H₃O⁺ ion pair, the indirect forming
26 process of HSO₄⁻···H₃O⁺ ion pair required more time. This was consistent with the interfacial
27 reactions of CH₂OO + HNO₃ (Kumar et al., 2018) and the hydration of SO₃ (Lv and Sun, 2020)
28 where the direct forming mechanism needed less time than indirect forming mechanism.

29 ***The H₂S₂O₇ Dissociating on Water Droplet.*** In addition to the gaseous SO₃ colliding with SA⁻
30 at the air-water interface, DSA, the product of the barrierless reaction between SO₃ and SA, can

1 further quickly react with interfacial water molecule at the air-water interface. As seen in Fig. 4,
 2 Fig. S7 and Movie S4, DSA was highly reactive at the air-water interface and can undergo two
 3 deprotonations to form $\text{S}_2\text{O}_7^{2-}$ ion. Specifically, the DSA can firstly form a H-bond with interfacial
 4 water molecule at 0.45 ps. After that, the H1 atom of DSA transferred to interfacial water and
 5 produced HS_2O_7^- and H_3O^+ ions. The formed HS_2O_7^- ion can survive for ~ 3 ps on water droplet. At
 6 4.14 ps, the H2 atom of HS_2O_7^- ion moved to O4 atom of nearby interfacial water molecule and
 7 produced the formation of $\text{S}_2\text{O}_7^{2-}\cdots\text{H}_3\text{O}^+$ ion pair, which was stable at the air-water interface over a
 8 simulated time scale of 10 ps. Note that the second deprotonation of DSA indeed needs more time
 9 than its first deprotonation as the $\text{p}K_{a1}$ ($\text{p}K_{a1} = -16.05$) of DSA is much smaller than its $\text{p}K_{a2}$ ($\text{p}K_{a2}$
 10 $= -4.81$) (Abedi and Farrokhpour, 2013). In brief, at the air-water interface, both these two routes of
 11 the formation of $\text{S}_2\text{O}_7^{2-}\cdots\text{H}_3\text{O}^+$ ion pair occurred on the picosecond time scale.

12 3.3 Atmospheric Implications

13 *The application of the $\text{SO}_3 + \text{SA}$ reaction in atmospheric chemistry.* In the gas-phase, the
 14 main sink route of SO_3 was H_2O -assisted hydrolysis of SO_3 (Morokuma and Muguruma, 1994;
 15 Akhmatskaya et al., 1997; Larson et al., 2000; Hazra and Sinha, 2011; Long et al., 2013a; Torrent-
 16 Sucarrat et al., 2012; Ma et al., 2020). To study the atmospheric importance of the $\text{SO}_3 + \text{SA}$ reaction
 17 without and with H_2O , the rate ratio ($v_{\text{DSA}}/v_{\text{SA}}$) between the $\text{SO}_3 + \text{SA}$ reaction and H_2O -assisted
 18 hydrolysis of SO_3 was compared, which was expressed in Eq. (5).

$$19 \frac{v_{\text{DSA}}}{v_{\text{SA}}} = \frac{k_{\text{DSA}} \times [\text{SO}_3] \times [\text{H}_2\text{SO}_4] + k_{\text{DSA_WM_s}} \times K_{\text{eq1}} \times [\text{SO}_3] \times [\text{H}_2\text{SO}_4] \times [\text{H}_2\text{O}]}{k_{\text{SA_WM}} \times K_{\text{eq2}} \times [\text{SO}_3] \times [\text{H}_2\text{O}] \times [\text{H}_2\text{O}]} \quad (5)$$

20 In Eq. (5), K_{eq1} and K_{eq2} were the equilibrium constant for the formation of $\text{H}_2\text{SO}_4\cdots\text{H}_2\text{O}$ and
 21 $\text{SO}_3\cdots\text{H}_2\text{O}$ complexes shown in Table S2, respectively; k_{DSA} , $k_{\text{DSA_WM_s}}$ and $k_{\text{SA_WM}}$ were
 22 respectively denoted the bimolecular rate coefficient for the $\text{H}_2\text{SO}_4 + \text{SO}_3$, $\text{H}_2\text{SO}_4\cdots\text{H}_2\text{O} + \text{SO}_3$ and
 23 $\text{SO}_3\cdots\text{H}_2\text{O} + \text{H}_2\text{O}$ reactions; $[\text{H}_2\text{O}]$ and $[\text{H}_2\text{SO}_4]$ were respectively represented the concentration of
 24 H_2O and SA taken from references (Anglada et al., 2013; Liu et al., 2015); The value of $v_{\text{DSA}}/v_{\text{SA}}$
 25 was listed in Table S7 (0 km altitude) and Table S8 (5-30 km altitude). As seen in Table S7, the
 26 hydrolysis reaction of SO_3 with $(\text{H}_2\text{O})_2$ was more favorable than the $\text{SO}_3 + \text{H}_2\text{SO}_4$ reaction at 0 km
 27 altitude as the $[\text{H}_2\text{O}]$ (10^{16} - 10^{18} molecules $\cdot\text{cm}^3$) was much larger than that of $[\text{H}_2\text{SO}_4]$ (10^4 - 10^8
 28 molecules $\cdot\text{cm}^3$). Although the concentration of water molecules decreased with the increasing of
 29 altitude in Table S8, the concentration of $[\text{H}_2\text{O}]$ was still much greater than that of $[\text{H}_2\text{SO}_4]$, resulting

1 in the $\text{SO}_3 + \text{H}_2\text{SO}_4$ reaction cannot compete with H_2O -assisted hydrolysis of SO_3 within the altitude
2 range of 5-30 km. Even considering of high H_2SO_4 concentration at the end and outside the aircraft
3 engine and flight at 10 km (Curtius et al., 2002), the $\text{SO}_3 + \text{H}_2\text{SO}_4$ reaction was not the major sink
4 route of SO_3 . Notably, as the concentration of sulfuric acid was even greater than that of water vapor
5 in the atmosphere of Venus, the $\text{SO}_3 + \text{SA}$ reaction was probably favorable than the H_2O -assisted
6 hydrolysis of SO_3 in the Venus' atmosphere. To check whether the $\text{SO}_3 + \text{H}_2\text{SO}_4$ reaction was more
7 favorable than H_2O -assisted hydrolysis of SO_3 or not in the Venus' atmosphere, the rate ratio of
8 $v_{\text{DSA}}/v_{\text{SA}}$ listed in Eq. 4 has been calculated in Table 2. It can be seen from Table 2 that the rate ratio
9 of $v_{\text{DSA}}/v_{\text{SA}}$ was 3.24×10^8 - 5.23×10^{10} within the altitude range of 40-70 km in the Venus'
10 atmosphere, which indicates that the $\text{SO}_3 + \text{H}_2\text{SO}_4$ reaction is significantly more favorable than the
11 hydrolysis reaction of $\text{SO}_3 + (\text{H}_2\text{O})_2$ within the altitudes range of 40-70 km in the Venus' atmosphere.

12 **Enhancement Effect of DSA on NPF.** From the multistep global minimum sampling
13 technique, for $(\text{DSA})_x(\text{SA})_y(\text{A})_z$ ($z \leq x + y \leq 3$) molecular clusters, 27 most stable structures in the
14 present system have been found (Fig. S11). To evaluate the thermodynamic stability of these
15 clusters, Gibbs formation free energies (ΔG) at 278.15 K and evaporation rate coefficient (γ , s^{-1}) for
16 $(\text{DSA})_x(\text{SA})_y(\text{A})_z$ ($z \leq x + y \leq 3$) molecular clusters were calculated in Fig. 5 and Table S11-12,
17 respectively. As for dimers formed by SA, A and DSA, the ΔG of $(\text{A})_1 \cdot (\text{DSA})_1$ was $-16.1 \text{ kcal} \cdot \text{mol}^{-1}$,
18 ¹, which was lowest in all dimers followed by $(\text{SA})_2$ ($-8.5 \text{ kcal} \cdot \text{mol}^{-1}$) and then $(\text{SA})_1 \cdot (\text{A})_1$ (-6.3
19 $\text{ kcal} \cdot \text{mol}^{-1}$), meanwhile, the γ of $(\text{A})_1 \cdot (\text{DSA})_1$ ($1.17 \times 10^{-3} \text{ s}^{-1}$) was lower than those of $(\text{SA})_2$ (3.81
20 $\times 10^2 \text{ s}^{-1}$) and $(\text{SA})_1 \cdot (\text{A})_1$ ($4.19 \times 10^4 \text{ s}^{-1}$). Regarding for the SA-A-DSA-based clusters, the values
21 of ΔG and γ of SA-A-DSA-based clusters containing more DSA molecules were relatively lower
22 than the corresponding values of other SA-A-DSA-based clusters with the same number of acid and
23 base molecules. In the free-energy diagram for cluster formation steps of the SA-A-DSA system
24 (Fig. 5), thermodynamic barriers were weakened mainly by the subsequential addition of A or DSA
25 monomer. Also, the SA-A-DSA-based growth pathway was thermodynamically favorable with
26 decreasing ΔG . These results indicate that DSA not only can promote the stability of SA-A-DSA-
27 based clusters but also may synergistically participate in the nucleation process.

28 The potential enhancement influence of DSA to the SA-A-based particle formation was shown
29 in Fig. 6. The formation rate (J , $\text{cm}^{-3} \cdot \text{s}^{-1}$) of SA-A-DSA-based system illustrated in Fig. 6 was
30 negatively dependent on temperature, demonstrating that the low temperature is a key factor to

1 accelerate cluster formation. It is noted that, at low temperatures of 218.15 K (Fig. S12) and 238.15
2 K (Fig. S13), the actual ΔG of clusters has been calculated to ensure meaningful cluster dynamics
3 of the 3×3 systems, where the actual ΔG surface represented that the simulated set of clusters
4 always included the critical cluster. In addition to temperature, the J of SA-A-DNA-based system
5 shown in Fig. 6 rise with the increase of [DNA]. More notably, the participation of DNA can promote
6 J to a higher level, indicating its enhancement on SA-A nucleation. Besides, there was significantly
7 positive dependence of the J of SA-A-DNA-based system on both [SA] and [A] in Fig. 7 (238.15
8 K) and Fig. S15-Fig. S18 (218.15, 258.15, 278.15 and 298.15 K). This was because the higher
9 concentration of nucleation precursors could lead to higher J . Besides, Fig. S19 showed the
10 nucleation rate when the sum ($[SA] + [DNA]$) was kept constant. $J_{DNA/SA}$ at substituted condition
11 was higher than that at unsubstituted condition. These results indicated that DNA may can greatly
12 enhance the SA-A particle nucleation in heavy sulfur oxide polluted atmospheric boundary layer,
13 especially at an average flight altitude of 10 km with high [DNA].

14 Two main cluster formation pathways, the pure SA-A-based cluster (*i*) and DNA-containing
15 cluster (*ii*), at different [DNA] and different temperatures (218.15 K, 238.15 K and 258.15 K) were
16 shown in Fig. 8(a). As seen, the DNA molecule exhibited an ability to directly participate in cluster
17 formation under high [SA] and [DNA], and median [A]. Interestingly, at different temperature and
18 different [DNA], the DNA molecule showed different effect mechanism and contribution in SA-A
19 system. As seen in Fig. 8(b) and Fig. S20(b), the cluster growth pathways were dominated by DNA-
20 containing cluster formation under the conditions of 238.15 K ([DNA] is 10^6 - 10^7 molecules·cm⁻³),
21 258.15 K ([DNA] is 10^5 - 10^7 molecules·cm⁻³), 278.15 K ([DNA] is 10^4 - 10^7 molecules·cm⁻³) and
22 298.15 K ([DNA] is 10^4 - 10^7 molecules·cm⁻³). By the way, the cluster growth pathways were
23 completely dominated by the DNA-containing cluster at 298.15 K where [DNA]= 10^5 - 10^7
24 molecules·cm⁻³, and its contribution for growth flux out of the system reached to 100% (Fig. S22).
25 In short, on one hand, the contribution of the DNA participation pathway has been increased with
26 increasing temperature. On the other hand, the contribution of the pathway with participation of
27 DNA increased with increasing [DNA], while the number of DNA molecules contained in clusters
28 $[(SA)_2 \cdot (A)_3 \cdot DNA, SA \cdot (A)_2 \cdot DNA, SA \cdot (A)_3 \cdot (DNA)_2, \text{ and } (A)_3 \cdot (DNA)_3]$ that can contribute to cluster
29 growth had a positive correlation with [DNA]. These results suggested that DNA has the ability to
30 act as a potential contributor to SA-A-based NPF in the atmosphere at low T , low [SA], high [A]

1 and high [DSA], and the DSA participation pathway can be dominant in heavy sulfur oxide polluted
2 atmospheric boundary layer and in season of late autumn and early winter.

3 At the air-water interface, important implication of the BOMD simulations was that the
4 reaction between SO_3 and SA at the air-water interface can be accomplished within a few
5 picoseconds, among which the interfacial water molecules played a significant role in promoting
6 the formation of $\text{S}_2\text{O}_7^{2-}\cdots\text{H}_3\text{O}^+$ and $\text{SA}^-\cdots\text{H}_3\text{O}^+$ ion pairs. Furthermore, the adsorption capacity of
7 the $\text{S}_2\text{O}_7^{2-}$, H_3O^+ and SA^- to gaseous precursors in the atmosphere was further investigated by the
8 calculated interaction free energies. Herein, the species of SA, NH_3 , HNO_3 and $(\text{COOH})_2$ have been
9 regarded as the candidate species. (Kulmala et al., 2004; Kirkby et al., 2011). Our calculated Gibbs
10 free energies in Table 3 showed that the interactions of $\text{S}_2\text{O}_7^{2-}\cdots\text{H}_2\text{SO}_4$, $\text{S}_2\text{O}_7^{2-}\cdots\text{HNO}_3$, $\text{S}_2\text{O}_7^{2-}$
11 $\cdots(\text{COOH})_2$, $\text{H}_3\text{O}^+\cdots\text{NH}_3$, $\text{H}_3\text{O}^+\cdots\text{H}_2\text{SO}_4$, $\text{SA}^-\cdots\text{H}_2\text{SO}_4$, $\text{SA}^-\cdots(\text{COOH})_2$, and $\text{SA}^-\cdots\text{HNO}_3$ were
12 stronger than those of $\text{H}_2\text{SO}_4\cdots\text{NH}_3$ (major precursor of atmospheric aerosols) with their binding
13 free energies enhanced by 18.6-42.8 $\text{kcal}\cdot\text{mol}^{-1}$. These results reveal that interfacial $\text{S}_2\text{O}_7^{2-}$, SA^- and
14 H_3O^+ can attract candidate species from the gas phase to the water surface. Moreover, we evaluated
15 the nucleation potential of $\text{S}_2\text{O}_7^{2-}$ on SA-A cluster by considering geometrical structure and the
16 formation free energies of the $(\text{SA})_1(\text{A})_1(\text{S}_2\text{O}_7^{2-})_1$ clusters. As compared with $(\text{SA})_1(\text{A})_1(\text{X})_1$ ($\text{X} =$
17 $\text{HOOCCH}_2\text{COOH}$, $\text{HOCCOOSO}_3\text{H}$, $\text{CH}_3\text{OSO}_3\text{H}$, $\text{HOOCCH}_2\text{CH}(\text{NH}_2)\text{COOH}$ and HOCH_2COOH)
18 clusters (Zhong et al., 2019; Zhang et al., 2018; Rong et al., 2020; Gao et al., 2023; Liu et al., 2021a;
19 Zhang et al., 2017), the number of hydrogen bonds in $(\text{SA})_1(\text{A})_1(\text{S}_2\text{O}_7^{2-})_1$ cluster presented in Fig.
20 S8 increased and the ring of the complex was enlarged. It was demonstrated that $\text{S}_2\text{O}_7^{2-}$ has the
21 highest potential to stabilize SA-A clusters and promote SA-A nucleation in these clusters due to its
22 acidity and structural factors such as more intermolecular hydrogen bond binding sites.
23 Subsequently, comparing to $(\text{SA})_1(\text{A})_1(\text{X})_1$ clusters (Table 2), the Gibbs formation free energy ΔG
24 of $(\text{SA})_1(\text{A})_1(\text{S}_2\text{O}_7^{2-})_1$ cluster was lower, showing $\text{S}_2\text{O}_7^{2-}$ ion at the air-water interface has stronger
25 nucleation ability than X in the gas phase. Therefore, we predict that $\text{S}_2\text{O}_7^{2-}$ at the air-water interface
26 has stronger nucleation potential.

27 4. Summary and Conclusions

28 In this work, we employed QC calculations, BOMD simulations and ACDC kinetic model to
29 characterize the SO_3 - H_2SO_4 interaction in the gas phase and at the air-water interface and to study

1 the effect of $\text{H}_2\text{S}_2\text{O}_7$ on $\text{H}_2\text{SO}_4\text{-NH}_3$ -based clusters. Results revealed that the energy barrier of the
2 gas phase $\text{SO}_3 + \text{H}_2\text{SO}_4$ reaction without and with H_2O was less than $2.3 \text{ kcal}\cdot\text{mol}^{-1}$. Rate constants
3 indicated that though the $\text{SO}_3 + \text{H}_2\text{SO}_4$ reaction cannot compete with H_2O -assisted hydrolysis of
4 SO_3 within the temperature range of 280-320 K, its rate constant was close to the upper limits for
5 bimolecular reactions and H_2O exerted obvious catalytic role in promoting the reaction rate.
6 Moreover, ACDC kinetic simulations showed that DSA has unexpected facilitate effects on the NPF
7 process and can present a more obvious enhancement effect on SA-A-based cluster formation in
8 polluted atmospheric boundary layer. Of particular note, DSA can directly participate in the SA-A-
9 based cluster formation pathway and the contribution of the pathway with participation of DSA
10 increases with increasing [DSA] in regions with atmospheric pollution boundary layer of high
11 concentrations of SO_3 , especially in late autumn and early winter.

12 At the air-water interface, H_2O -induced the formation of $\text{S}_2\text{O}_7^{2-}\cdots\text{H}_3\text{O}^+$ ion pair, SA^- mediated
13 the formation of $\text{SA}^-\cdots\text{H}_3\text{O}^+$ ion pair and the deprotonation of $\text{H}_2\text{S}_2\text{O}_7$ were observed, both of which
14 can occur within a few picoseconds. The formed interfacial $\text{S}_2\text{O}_7^{2-}$, SA^- and H_3O^+ can attract
15 candidate species (such as H_2SO_4 , NH_3 , and HNO_3) for particle formation from the gas phase to the
16 water surface, and thus accelerated the growth of particle. Moreover, potential of X ($X = \text{S}_2\text{O}_7^{2-}$,
17 $\text{HOOCCH}_2\text{COOH}$, $\text{HOCCOOSO}_3\text{H}$, $\text{CH}_3\text{OSO}_3\text{H}$, $\text{HOOCCH}_2\text{CH}(\text{NH}_2)\text{COOH}$ and HOCH_2COOH)
18 in ternary SA-A- X cluster formation indicated that $\text{S}_2\text{O}_7^{2-}$ has the highest potential to stabilize SA-
19 A clusters and promote SA-A nucleation among X .

20 The present work will expand our understanding of new pathway for the loss of SO_3 in acidic
21 polluted areas. Moreover, this work will also help to reveal some missing sources of metropolis
22 industrial regions NPF and to understand the atmospheric organic-sulfur cycle more
23 comprehensively.

24 **Acknowledgments**

25 This work was supported by the National Natural Science Foundation of China (No: 22203052;
26 22073059; 22006158); the Education Department of Shaanxi Provincial Government (no. 23JC023),
27 the Key Cultivation Project of Shaanxi University of Technology (No: SLG2101); The Special
28 Scientific Research Project of Hanzhong City-Shaanxi University of Technology Co-construction
29 State Key Laboratory (SXJ-2106); The authors thank Prof. Qingzhu Zhang and Fei Xu from
30 Shandong University for their sincere assistance in calculating the air-water interface reaction.

1 Declaration of competing interest

2 The authors declare that they have no known competing financial interests or personal
3 relationships that could have appeared to influence the work reported in this paper.

4 Reference

- 5 Abedi, M., and Farrokhpour, H.: Acidity constants of some sulfur oxoacids in aqueous solution using
6 CCSD and MP2 methods, *Dalton Trans.*, 42, 5566-5572, 10.1039/C3DT33056G, 2013.
- 7 Adler, T. B., Knizia, G., and Werner, H. J.: A simple and efficient CCSD(T)-F12 approximation, *J. Chem.*
8 *Phys.*, 127, 221106, 10.1063/1.2817618, 2007.
- 9 Akhmatkaya, E., Apps, C., Hillier, I., Masters, A., Palmer, I., Watt, N., Vincent, M., and Whitehead, J.:
10 Hydrolysis of SO₃ and ClONO₂ in water clusters A combined experimental and theoretical study, *J.*
11 *Am. Chem. Soc.*, 93, 2775-2779, 1997.
- 12 Almeida, J., Schobesberger, S., Kürten, A., Ortega, I. K., Kupiainen-Määttä, O., Praplan, A. P., Adamov,
13 A., Amorim, A., Bianchi, F., Breitenlechner, M., David, A., Dommen, J., Donahue, N. M., Downard,
14 A., Dunne, E., Duplissy, J., Ehrhart, S., Flagan, R. C., Franchin, A., Guida, R., Hakala, J., Hansel,
15 A., Heinritzi, M., Henschel, H., Jokinen, T., Junninen, H., Kajos, M., Kangasluoma, J., Keskinen,
16 H., Kupc, A., Kurtén, T., Kvashin, A. N., Laaksonen, A., Lehtipalo, K., Leiminger, M., Leppä, J.,
17 Loukonen, V., Makhmutov, V., Mathot, S., McGrath, M. J., Nieminen, T., Olenius, T., Onnela, A.,
18 Petäjä, T., Riccobono, F., Riipinen, I., Rissanen, M., Rondo, L., Ruuskanen, T., Santos, F. D., Sarnela,
19 N., Schallhart, S., Schnitzhofer, R., Seinfeld, J. H., Simon, M., Sipilä, M., Stozhkov, Y., Stratmann,
20 F., Tomé, A., Tröstl, J., Tsagkogeorgas, G., Vaattovaara, P., Viisanen, Y., Virtanen, A., Vrtala, A.,
21 Wagner, P. E., Weingartner, E., Wex, H., Williamson, C., Wimmer, D., Ye, P., Yli-Juuti, T., Carslaw,
22 K. S., Kulmala, M., Curtius, J., Baltensperger, U., Worsnop, D. R., Vehkamäki, H., and Kirkby, J.:
23 Molecular understanding of sulphuric acid–amine particle nucleation in the atmosphere, *Nature*,
24 502, 359-363, 10.1038/nature12663, 2013.
- 25 Anglada, J. M., Hoffman, G. J., Slipchenko, L. V., M. Costa, M., Ruiz-Lopez, M. F., and Francisco, J. S.:
26 Atmospheric significance of water clusters and ozone-water complexes, *J. Phys. Chem. A*, 117,
27 10381-10396, 2013.
- 28 Bandyopadhyay, B., Kumar, P., and Biswas, P.: Ammonia Catalyzed Formation of Sulfuric Acid in
29 Troposphere: The Curious Case of a Base Promoting Acid Rain, *J. Phys. Chem. A*, 121, 3101-3108,
30 10.1021/acs.jpca.7b01172, 2017.
- 31 Becke, A. D.: Density-functional exchange-energy approximation with correct asymptotic behavior,
32 *Phys. Rev. A*, 38, 3098-3100, 1988.
- 33 Bouo, F.-X., Kouamé, J., Tchétché, Y., Kré, R., Moussé, M., Assamoi, P., Cautenet, S., and Cautenet, G.:
34 Redistribution of free tropospheric chemical species over West Africa: Radicals (OH and HO₂),
35 peroxide (H₂O₂) and acids (HNO₃ and H₂SO₄), *Chemosphere*, 84, 1617-1629, 2011.
- 36 Calvert, J. G., Lazrus, A., Kok, G. L., Heikes, B. G., Walega, J. G., Lind, J., and Cantrell, C. A.: Chemical
37 mechanisms of acid generation in the troposphere, *Nature*, 317, 27-35, 1985.
- 38 Cao, Y., Zhou, H., Jiang, W., Chen, C. W., and Pan, W. P.: Studies of the fate of sulfur trioxide in coal-
39 fired utility boilers based on modified selected condensation methods, *Environ. Sci. Technol.*, 44,
40 3429-3434, 2010.
- 41 Chen, L., and Bhattacharya, S.: Sulfur emission from Victorian brown coal under pyrolysis, oxy-fuel
42 combustion and gasification conditions, *Environ. Sci. Technol.*, 47, 1729-1734, 2013.

1 Chen, T., and Plummer, P. L.: Ab initio MO investigation of the gas-phase reaction sulfur trioxide + water.
2 fwdarw. sulfuric acid, *J. Phys. Chem. A*, 89, 3689-3693, 1985.

3 Chen, X., Tao, C., Zhong, L., Gao, Y., Yao, W., and Li, S.: Theoretical study on the atmospheric reaction
4 of SO₂ with the HO₂ and HO₂·H₂O complex formation HSO₄ and H₂SO₃, *Chem. Phys. Lett.*, 608,
5 272-276, 2014.

6 Cheng, Y., Ding, C., Wang, H., Zhang, T., Wang, R., Muthiah, B., Xu, H., Zhang, Q., and Jiang, M.:
7 Significant influence of water molecules on the SO₃ + HCl reaction in the gas phase and at the air-
8 water interface, *Phys. Chem. Chem. Phys.*, 25, 28885-28894, 10.1039/D3CP03172A, 2023.

9 Curtius, J., Arnold, F., and Schulte, P.: Sulfuric acid measurements in the exhaust plume of a jet aircraft
10 in flight: Implications for the sulfuric acid formation efficiency, *Geophys. Res. Lett.*, 29, 17-11-17-
11 14, 2002.

12 Elm, J., Bilde, M., and Mikkelsen, K. V.: Assessment of density functional theory in predicting structures
13 and free energies of reaction of atmospheric prenucleation clusters, *J. Chem. Theory Comput.*, 8,
14 2071-2077, 2012.

15 Elm, J., Bilde, M., and Mikkelsen, K. V.: Influence of nucleation precursors on the reaction kinetics of
16 methanol with the OH radical, *J. Phys. Chem. A*, 117, 6695-6701, 2013.

17 England, G. C., Zielinska, B., Loos, K., Crane, I., and Ritter, K.: Characterizing PM_{2.5} emission profiles
18 for stationary sources: comparison of traditional and dilution sampling techniques, *Fuel Process.*
19 *Technol.*, 65, 177-188, 2000.

20 Finlayson-Pitts, B. J., and Pitts Jr, J. N.: Atmospheric chemistry. Fundamentals and experimental
21 techniques, John Wiley and Sons: New York, 1986.

22 Frisch, M. J., Trucks, G. W., Schlegel, H. B., Scuseria, G. E., Robb, M. A., Cheeseman, J. R., Scalmani,
23 G., Barone, V., Mennucci, B., Petersson, G. A., Nakatsuji, H., Caricato, M., Li, X., Hratchian, H. P.,
24 Izmaylov, A. F., Bloino, J., Zheng, G., Sonnenberg, J. L., Hada, M., Ehara, M., Toyota, K., Fukuda,
25 R., Hasegawa, J., Ishida, M., Nakajima, T., Honda, Y., Kitao, O., Nakai, H., Vreven, T., Montgomery,
26 J. A., Jr., Peralta, J. E., Ogliaro, F., Bearpark, M., Heyd, J. J., Brothers, E., Kudin, K. N., Staroverov,
27 V. N., Kobayashi, R., Normand, J., Raghavachari, K., Rendell, A., Burant, J. C., Iyengar, S. S.,
28 Tomasi, J., Cossi, M., Rega, N., Millam, J. M., Klene, M., Knox, J. E., Cross, J. B., Bakken, V.,
29 Adamo, C., Jaramillo, J., Gomperts, R., Stratmann, R. E., Yazyev, O., Austin, A. J., Cammi, R.,
30 Pomelli, C., Ochterski, J. W., Martin, R. L., Morokuma, K., Zakrzewski, V. G., Voth, G. A., Salvador,
31 P., Dannenberg, J. J., Dapprich, S., Daniels, A. D., Farkas, Ö., Foresman, J. B., Ortiz, J. V.,
32 Cioslowski, J., and Fox, D. J: Gaussian09 Revision D. 01, Gaussian Inc. Wallingford CT, See also:
33 URL: <http://www.gaussian.com>, 2009.

34 Gao, J., Wang, R., Zhang, T., Liu, F., and Wang, W.: Effect of methyl hydrogen sulfate on the formation
35 of sulfuric acid-ammonia clusters: A theoretical study, *J. Chin. Chem. Soc.*, 70, 689-698,
36 <https://doi.org/10.1002/jccs.202200148>, 2023.

37 Glowacki, D. R., Liang, C.-H., Morley, C., Pilling, M. J., and Robertson, S. H.: MESMER: an open-
38 source master equation solver for multi-energy well reactions, *J. Phys. Chem. A*, 116, 9545-9560,
39 2012.

40 Goedecker, S., Teter, M., and Hutter, J.: Separable dual-space Gaussian pseudopotentials, *Phys. Rev. B*,
41 54, 1703, 1996.

42 Gonzalez, J., Torrent-Sucarrat, M., and Anglada, J. M.: The reactions of SO₃ with HO₂ radical and
43 H₂O···HO₂ radical complex. Theoretical study on the atmospheric formation of HSO₅ and H₂SO₄,
44 *Phys. Chem. Chem. Phys.*, 12, 2116-2125, 2010.

1 Grimme, S., Antony, J., Ehrlich, S., and Krieg, H.: A consistent and accurate ab initio parametrization of
2 density functional dispersion correction (DFT-D) for the 94 elements H-Pu, *J. Chem. Phys.*, 132,
3 154104, 2010.

4 Hartwigsen, C., Goedecker, S., and Hutter, J.: Relativistic separable dual-space Gaussian
5 pseudopotentials from H to Rn, *Phys. Rev. B*, 58, 3641-3662, 1998.

6 Haywood, J., and Boucher, O.: Estimates of the direct and indirect radiative forcing due to tropospheric
7 aerosols: A review, *Rev. Geophys.*, 38, 513-543, 2000.

8 Hazra, M. K., and Sinha, A.: Formic acid catalyzed hydrolysis of SO₃ in the gas phase: A barrierless
9 mechanism for sulfuric acid production of potential atmospheric importance, *J. Am. Chem. Soc.*,
10 133, 17444-17453, 2011.

11 Hofmann, M., and Schleyer, P. v. R.: Acid rain: Ab initio investigation of the H₂O•SO₃ complex and its
12 conversion to H₂SO₄, *J. Am. Chem. Soc.*, 116, 4947-4952, 1994.

13 Horváth, G., Horváth, I., Almousa, S. A.-D., and Telek, M.: Numerical inverse Laplace transformation
14 using concentrated matrix exponential distributions, *Perform. Evaluation*, 137, 102067, 2020.

15 Huff, A. K., Mackenzie, R. B., Smith, C. J., and Leopold, K. R.: Facile Formation of Acetic Sulfuric
16 Anhydride: Microwave Spectrum, Internal Rotation, and Theoretical Calculations, *J. Phys. Chem.*
17 *A*, 121, 5659-5664, 10.1021/acs.jpca.7b05105, 2017.

18 Hutter, J., Iannuzzi, M., Schiffmann, F., and VandeVondele, J.: Wiley Interdiscip, *Wiley Interdiscip. Rev.*
19 *Comput. Mol. Sci.*, 4, 15-25, 2014.

20 Kanno, N., Tonokura, K., and Koshi, M.: Equilibrium constant of the HO₂-H₂O complex formation and
21 kinetics of HO₂ + HO₂-H₂O: Implications for tropospheric chemistry, *J. Geophys. Res.: Atmos.*, 111,
22 10.1029/2005jd006805, 2006.

23 Kikuchi, R.: Environmental management of sulfur trioxide emission: impact of SO₃ on human health,
24 *Environ. Manage.*, 27, 837-844, 2001.

25 Kirkby, J., Curtius, J., Almeida, J., Dunne, E., Duplissy, J., Ehrhart, S., Franchin, A., Gagné, S., Ickes,
26 L., Kürten, A., Kupc, A., Metzger, A., Riccobono, F., Rondo, L., Schobesberger, S., Tsagkogeorgas,
27 G., Wimmer, D., Amorim, A., Bianchi, F., Breitenlechner, M., David, A., Dommen, J., Downard, A.,
28 Ehn, M., Flagan, R. C., Haider, S., Hansel, A., Hauser, D., Jud, W., Junninen, H., Kreissl, F., Kvashin,
29 A., Laaksonen, A., Lehtipalo, K., Lima, J., Lovejoy, E. R., Makhmutov, V., Mathot, S., Mikkilä, J.,
30 Minginette, P., Mogo, S., Nieminen, T., Onnela, A., Pereira, P., Petäjä, T., Schnitzhofer, R., Seinfeld,
31 J. H., Sipilä, M., Stozhkov, Y., Stratmann, F., Tomé, A., Vanhanen, J., Viisanen, Y., Vrtala, A.,
32 Wagner, P. E., Walther, H., Weingartner, E., Wex, H., Winkler, P. M., Carslaw, K. S., Worsnop, D.
33 R., Baltensperger, U., and Kulmala, M.: Role of sulphuric acid, ammonia and galactic cosmic rays
34 in atmospheric aerosol nucleation, *Nature*, 476, 429-433, 10.1038/nature10343, 2011.

35 Knizia, G., Adler, T. B., and Werner, H.-J.: Simplified CCSD(T)-F12 methods: Theory and benchmarks,
36 *J. Chem. Phys.*, 130, 054104, 10.1063/1.3054300, 2009.

37 Kuang, C., McMurry, P. H., McCormick, A. V., and Eisele, F.: Dependence of nucleation rates on sulfuric
38 acid vapor concentration in diverse atmospheric locations, *J. Geophys. Res. Atmos.*, 113, 2008.

39 Kuczkowski, R. L., Suenram, R. D., and Lovas, F. J.: Microwave spectrum, structure, and dipole moment
40 of sulfuric acid, *J. Am. Chem. Soc.*, 103, 2561-2566, 1981.

41 Kulmala, M., Vehkamäki, H., Petäjä, T., Dal Maso, M., Lauri, A., Kerminen, V. M., Birmili, W., and
42 McMurry, P. H.: Formation and growth rates of ultrafine atmospheric particles: a review of
43 observations, *J. Aerosol Sci.*, 35, 143-176, <https://doi.org/10.1016/j.jaerosci.2003.10.003>, 2004.

1 Kumar, M., Zhong, J., Francisco, J. S., and Zeng, X. C.: Criegee intermediate-hydrogen sulfide chemistry
2 at the air/water interface, *Chem. Sci.*, 8, 5385-5391, 2017.

3 Kumar, M., Zhong, J., Zeng, X. C., and Francisco, J. S.: Reaction of Criegee Intermediate with Nitric
4 Acid at the Air-Water Interface, *J. Am. Chem. Soc.*, 140, 4913-4921, 10.1021/jacs.8b01191, 2018.

5 Larson, L. J., Kuno, M., and Tao, F.-M.: Hydrolysis of sulfur trioxide to form sulfuric acid in small water
6 clusters, *J. Chem. Phys.*, 112, 8830-8838, 2000.

7 Lee, C., Yang, W., and Parr, R. G.: Development of the Colle-Salvetti correlation-energy formula into a
8 functional of the electron density, *Phys. Rev. B*, 37, 785-789, 1988.

9 Li, H., Zhong, J., Vehkamäki, H., Kurtén, T., Wang, W., Ge, M., Zhang, S., Li, Z., Zhang, X., Francisco,
10 J. S., and Zeng, X. C.: Self-Catalytic Reaction of SO₃ and NH₃ To Produce Sulfamic Acid and Its
11 Implication to Atmospheric Particle Formation, *J. Am. Chem. Soc.*, 140, 11020-11028,
12 10.1021/jacs.8b04928, 2018a.

13 Li, K., Song, X., Zhu, T., Wang, C., Sun, X., Ning, P., and Tang, L.: Mechanistic and kinetic study on the
14 catalytic hydrolysis of COS in small clusters of sulfuric acid, *Environ. Pollut.*, 232, 615-623,
15 10.1016/j.envpol.2017.10.004, 2018b.

16 Li, L., Kumar, M., Zhu, C., Zhong, J., Francisco, J. S., and Zeng, X. C.: Near-barrierless ammonium
17 bisulfate formation via a loop-structure promoted proton-transfer mechanism on the surface of water,
18 *J. Am. Chem. Soc.*, 138, 1816-1819, 2016.

19 Liu, J., Fang, S., Wang, Z., Yi, W., Tao, F. M., and Liu, J. Y.: Hydrolysis of sulfur dioxide in small clusters
20 of sulfuric acid: Mechanistic and kinetic study, *Environ. Sci. Technol.*, 49, 13112-13120, 2015.

21 Liu, J., Liu, L., Rong, H., and Zhang, X.: The potential mechanism of atmospheric new particle formation
22 involving amino acids with multiple functional groups, *Phys. Chem. Chem. Phys.*, 23, 10184-10195,
23 10.1039/D0CP06472F, 2021a.

24 Liu, L., Zhong, J., Vehkamäki, H., Kurtén, T., Du, L., Zhang, X., Francisco, J. S., and Zeng, X. C.:
25 Unexpected quenching effect on new particle formation from the atmospheric reaction of methanol
26 with SO₃, *Proc. Natl. Acad. Sci. U.S.A.*, 116, 24966-24971, 2019.

27 Liu, L., Yu, F., Tu, K., Yang, Z., and Zhang, X.: Influence of atmospheric conditions on the role of
28 trifluoroacetic acid in atmospheric sulfuric acid-dimethylamine nucleation, *Atmos. Chem. Phys.*, 21,
29 6221-6230, 10.5194/acp-21-6221-2021, 2021b.

30 Loerting, T., and Liedl, K. R.: Toward elimination of discrepancies between theory and experiment: The
31 rate constant of the atmospheric conversion of SO₃ to H₂SO₄, *Proc. Natl. Acad. Sci. U. S. A.*, 97,
32 8874-8878, 2000.

33 Lohmann, U., and Feichter, J.: Global indirect aerosol effects: a review, *J. Atmos. Chem. Phys.*, 5, 715-
34 737, 2005.

35 Long, B., Long, Z. W., Wang, Y.-b., Tan, X. F., Han, Y. H., Long, C. Y., Qin, S. J., and Zhang, W. J.:
36 Formic Acid Catalyzed Gas-Phase Reaction of H₂O with SO₃ and the Reverse Reaction: A
37 Theoretical Study, *ChemPhysChem*, 13, 323-329, 10.1002/cphc.201100558, 2012.

38 Long, B., Chang, C. R., Long, Z. W., Wang, Y. B., Tan, X. F., and Zhang, W. J.: Nitric acid catalyzed
39 hydrolysis of SO₃ in the formation of sulfuric acid: A theoretical study, *Chem. Phys. Lett.*, 581, 26-
40 29, 2013a.

41 Long, B., Tan, X. F., Chang, C. R., Zhao, W. X., Long, Z. W., Ren, D. S., and Zhang, W. J.: Theoretical
42 studies on gas-phase reactions of sulfuric acid catalyzed hydrolysis of formaldehyde and
43 formaldehyde with sulfuric acid and H₂SO₄·H₂O complex, *J. Phys. Chem. A* 117, 5106-5116,
44 2013b.

1 Lv, G., and Sun, X. M.: The role of air-water interface in the SO₃ hydration reaction, 230, 117514, 2020.

2 Lv, G., Sun, X., Zhang, C., and Li, M.: Understanding the catalytic role of oxalic acid in SO₃ hydration
3 to form H₂SO₄ in the atmosphere, *Atmos. Chem. Phys.*, 19, 2833-2844, 2019.

4 Ma, X., Zhao, X., Ding, Z., Wang, W., Wei, Y., Xu, F., Zhang, Q., and Wang, W.: Determination of the
5 amine-catalyzed SO₃ hydrolysis mechanism in the gas phase and at the air-water interface,
6 *Chemosphere*, 252, 126292, 2020.

7 Mackenzie, R. B., Dewberry, C. T., and Leopold, K. R.: Gas phase observation and microwave
8 spectroscopic characterization of formic sulfuric anhydride, *Science*, 349, 58-61, 2015.

9 MacKerell, A. D., Bashford, D., Bellott, M., Dunbrack, R. L., Evanseck, J. D., Field, M. J., Fischer, S.,
10 Gao, J., Guo, H., Ha, S., Joseph-McCarthy, D., Kuchnir, L., Kuczera, K., Lau, F. T. K., Mattos, C.,
11 Michnick, S., Ngo, T., Nguyen, D. T., Prodhom, B., Reiher, W. E., Roux, B., Schlenkrich, M., Smith,
12 J. C., Stote, R., Straub, J., Watanabe, M., Wiórkiewicz-Kuczera, J., Yin, D., and Karplus, M.: All-
13 Atom Empirical Potential for Molecular Modeling and Dynamics Studies of Proteins, *J. Phys. Chem.*
14 *B*, 102, 3586-3616, 10.1021/jp973084f, 1998.

15 Mardirossian, N., and Head-Gordon, M.: How accurate are the Minnesota density functionals for
16 noncovalent interactions, isomerization energies, thermochemistry, and barrier heights involving
17 molecules composed of main-group elements?, *J. Chem. Theory Comput.*, 12, 4303-4325, 2016.

18 McGrath, M. J., Olenius, T., Ortega, I. K., Loukonen, V., Paasonen, P., Kurtén, T., Kulmala, M., and
19 Vehkamäki, H.: Atmospheric Cluster Dynamics Code: a flexible method for solution of the birth-
20 death equations, *Atmos. Chem. Phys.*, 12, 2345-2355, 10.5194/acp-12-2345-2012, 2012.

21 Miller, J. A., and Klippenstein, S. J.: Master equation methods in gas phase chemical kinetics, *J. Phys.*
22 *Chem. A*, 110, 10528-10544, 2006.

23 Mitsui, Y., Imada, N., Kikkawa, H., and Katagawa, A.: Study of Hg and SO₃ behavior in flue gas of oxy-
24 fuel combustion system, *Int. J. Greenhouse Gas Control*, 5, S143-S150, 2011.

25 Morokuma, K., and Muguruma, C.: Ab initio molecular orbital study of the mechanism of the gas phase
26 reaction SO₃ + H₂O: Importance of the second water molecule, *J. Am. Chem. Soc.*, 116, 10316-
27 10317, 1994.

28 Neese, F.: The ORCA program system, *WIREs Comput. Mol. Sci.*, 2, 73-78,
29 <https://doi.org/10.1002/wcms.81>, 2012.

30 Otto, A. H., and Steudel, R.: Gas-Phase Structures and Acidities of the Sulfur Oxoacids H₂S_nO₆ (*n* = 2-
31 4) and H₂S₂O₇, *Eur. J. Inorg. Chem.*, 2001, 3047-3054, 2001.

32 Pérez-Ríos, J., Ragole, S., Wang, J., and Greene, C. H.: Comparison of classical and quantal calculations
33 of helium three-body recombination, *J. Chem. Phys.*, 140, 044307, 2014.

34 Pöschl, U.: Atmospheric aerosols: composition, transformation, climate and health effects, *Angew.*
35 *Chem., Int. Ed. Engl.*, 44, 7520-7540, 2005.

36 Pöschl, U., and Shiraiwa, M.: Multiphase chemistry at the atmosphere-biosphere interface influencing
37 climate and public health in the anthropocene, *Chem. Rev.*, 115, 4440-4475, 2015.

38 Renard, J. J., Calidonna, S. E., and Henley, M. V.: Fate of ammonia in the atmosphere-a review for
39 applicability to hazardous releases, *J. Hazard. Mater.*, 108, 29-60, 2004.

40 Riipinen, I., Sihto, S.-L., Kulmala, M., Arnold, F., Dal Maso, M., Birmili, W., Saarnio, K., Teinilä, K.,
41 Kerminen, V.-M., and Laaksonen, A.: Connections between atmospheric sulphuric acid and new
42 particle formation during QUEST III-IV campaigns in Heidelberg and Hyytiälä, *Atmos. Chem.*
43 *Phys.*, 7, 1899-1914, 2007.

1 Rong, H., Liu, L., Liu, J., and Zhang, X.: Glyoxylic sulfuric anhydride from the gas-phase reaction
2 between glyoxylic acid and SO₃: a potential nucleation precursor, *J. Phys. Chem. A*, 124, 3261-
3 3268, 2020.

4 Shampine, L. F., and Reichelt, M. W.: The MATLAB ODE Suite, *J. Sci. Comput.*, 18, 1-22,
5 10.1137/s1064827594276424, 1997.

6 Sihto, S.-L., Kulmala, M., Kerminen, V.-M., Dal Maso, M., Petäjä, T., Riipinen, I., Korhonen, H., Arnold,
7 F., Janson, R., and Boy, M.: Atmospheric sulphuric acid and aerosol formation: implications from
8 atmospheric measurements for nucleation and early growth mechanisms, *Atmos. Chem. Phys.*, 6,
9 4079-4091, 2006.

10 Sipilä, M., Berndt, T., Petäjä, T., Brus, D., Vanhanen, J., Stratmann, F., Patokoski, J., Mauldin III, R. L.,
11 Hyvärinen, A.-P., and Lihavainen, H.: The role of sulfuric acid in atmospheric nucleation, *Science*,
12 327, 1243-1246, 2010.

13 Smith, C. J., Huff, A. K., Mackenzie, R. B., and Leopold, K. R.: Observation of Two Conformers of
14 Acrylic Sulfuric Anhydride by Microwave Spectroscopy, *J. Phys. Chem. A*, 121, 9074-9080,
15 10.1021/acs.jpca.7b09833, 2017.

16 Starik, A., Savel'Ev, A., Titova, N., Loukhovitskaya, E., and Schumann, U.: Effect of aerosol precursors
17 from gas turbine engines on the volatile sulfate aerosols and ion clusters formation in aircraft plumes,
18 *Phys. Chem. Chem. Phys.*, 6, 3426-3436, 2004.

19 Steudel, R.: Sulfuric acid from sulfur trioxide and water-a surprisingly complex reaction, *Angew. Chem.*
20 *Int. Ed. Engl.*, 34, 1313-1315, 1995.

21 Stewart, J.: MOPAC2016 Stewart computational chemistry. Colorado Springs, CO: OpenMOPAC, in,
22 2016.

23 Stewart, J. J.: Optimization of parameters for semiempirical methods VI: more modifications to the
24 NDDO approximations and re-optimization of parameters, *J Mol Model*, 19, 1-32, 10.1007/s00894-
25 012-1667-x, 2013.

26 Stewart, J. J. P.: Optimization of parameters for semiempirical methods V: Modification of NDDO
27 approximations and application to 70 elements, *Journal of Molecular Modeling*, 13, 1173-1213,
28 10.1007/s00894-007-0233-4, 2007.

29 Stone, D., and Rowley, D. M.: Kinetics of the gas phase HO₂ self-reaction: Effects of temperature,
30 pressure, water and methanol vapours, *Phys. Chem. Chem. Phys.*, 7, 2156-2163,
31 10.1039/B502673C, 2005.

32 Tan, X. F., Long, B., Ren, D. S., Zhang, W. J., Long, Z. W., and Mitchell, E.: Atmospheric chemistry of
33 CH₃CHO: the hydrolysis of CH₃CHO catalyzed by H₂SO₄, *Phys. Chem.Chem.Phys.*, 20, 7701-7709,
34 2018.

35 Tilgner, A., Schaefer, T., Alexander, B., Barth, M., Collett Jr, J. L., Fahey, K. M., Nenes, A., Pye, H. O.,
36 Herrmann, H., and McNeill, V. F.: Acidity and the multiphase chemistry of atmospheric aqueous
37 particles and clouds, *Atmos. Chem. Phys.*, 21, 13483-13536, 2021.

38 Torrent-Sucarrat, M., Francisco, J. S., and Anglada, J. M.: Sulfuric acid as autocatalyst in the formation
39 of sulfuric acid, *J. Am. Chem. Soc.*, 134, 20632-20644, 2012.

40 VandeVondele, J., and Hutter, J.: Gaussian basis sets for accurate calculations on molecular systems in
41 gas and condensed phases, *J. Chem. Phys.*, 127, 114105, 2007.

42 Viegas, L. P., and Varandas, A. J.: Can water be a catalyst on the HO₂ + H₂O + O₃ reactive cluster?, *Chem.*
43 *Phys.*, 399, 17-22, 2012.

- 1 Viegas, L. P., and Varandas, A. J.: The $\text{HO}_2 + (\text{H}_2\text{O})_n + \text{O}_3$ reaction: an overview and recent developments,
2 Eur. Phys. J. D, 70, 1-9, 2016.
- 3 Wayne, R. P.: Chemistry of Atmospheres. An Introduction to the Chemistry of the Atmospheres of Earth,
4 the Planets, and Their Satellites, 3rd Oxford University Press, 10.1021/ja004780n, 2000.
- 5 Weber, R., McMurry, P., Eisele, F., and Tanner, D.: Measurement of expected nucleation precursor
6 species and 3-500-nm diameter particles at Mauna Loa observatory, Hawaii, J. Atmos. Sci., 52,
7 2242-2257, 1995.
- 8 Weber, R., Marti, J., McMurry, P., Eisele, F., Tanner, D., and Jefferson, A.: Measured atmospheric new
9 particle formation rates: Implications for nucleation mechanisms, Chem. Eng. Commun., 151, 53-
10 64, 1996.
- 11 Weber, R., Chen, G., Davis, D., Mauldin III, R., Tanner, D., Eisele, F., Clarke, A., Thornton, D., and
12 Bandy, A.: Measurements of enhanced H_2SO_4 and 3-4 nm particles near a frontal cloud during the
13 First Aerosol Characterization Experiment (ACE 1), J. Geophys. Res. Atmos., 106, 24107-24117,
14 2001.
- 15 Yang, Y., Liu, L., Wang, H., and Zhang, X.: Molecular-Scale Mechanism of Sequential Reaction of
16 Oxalic Acid with SO_3 : Potential Participator in Atmospheric Aerosol Nucleation, J. Phys. Chem. A,
17 125, 4200-4208, 2021.
- 18 Yao, L., Garmash, O., Bianchi, F., Zheng, J., Yan, C., Kontkanen, J., Junninen, H., Mazon, S. B., Ehn,
19 M., Paasonen, P., Sipilä, M., Wang, M., Wang, X., Xiao, S., Chen, H., Lu, Y., Zhang, B., Wang, D.,
20 Fu, Q., Geng, F., Li, L., Wang, H., Qiao, L., Yang, X., Chen, J., Kerminen, V.-M., Petäjä, T., Worsnop,
21 D. R., Kulmala, M., and Wang, L.: Atmospheric new particle formation from sulfuric acid and
22 amines in a Chinese megacity, Science, 361, 278-281, doi:10.1126/science.aao4839, 2018.
- 23 Yao, L., Fan, X., Yan, C., Kurtén, T., Daellenbach, K. R., Li, C., Wang, Y., Guo, Y., Dada, L., Rissanen,
24 M. P., Cai, J., Tham, Y. J., Zha, Q., Zhang, S., Du, W., Yu, M., Zheng, F., Zhou, Y., Kontkanen, J.,
25 Chan, T., Shen, J., Kujansuu, J. T., Kangasluoma, J., Jiang, J., Wang, L., Worsnop, D. R., Petäjä, T.,
26 Kerminen, V. M., Liu, Y., Chu, B., He, H., Kulmala, M., and Bianchi, F.: Unprecedented Ambient
27 Sulfur Trioxide (SO_3) Detection: Possible Formation Mechanism and Atmospheric Implications,
28 Environ. Sci. Technol. Lett., 7, 809-818, 10.1021/acs.estlett.0c00615, 2020.
- 29 Zhao, Y., and Truhlar, D. G.: The M06 suite of density functionals for main group thermochemistry,
30 thermochemical kinetics, noncovalent interactions, excited states, and transition elements: two new
31 functionals and systematic testing of four M06-class functionals and 12 other functionals, Theor.
32 Chem. Acc., 120, 215-241, 2008.
- 33 Zhang, H., Kupiainen-Määttä, O., Zhang, X., Molinero, V., Zhang, Y., and Li, Z.: The enhancement
34 mechanism of glycolic acid on the formation of atmospheric sulfuric acid-ammonia molecular
35 clusters, J. Chem. Phys., 146, 184308, 10.1063/1.4982929, 2017.
- 36 Zhang, H., Li, H., Liu, L., Zhang, Y., Zhang, X., and Li, Z.: The potential role of malonic acid in the
37 atmospheric sulfuric acid-ammonia clusters formation, Chemosphere, 203, 26-33, 2018.
- 38 Zhang, J., and Dolg, M.: ABCluster: the artificial bee colony algorithm for cluster global optimization,
39 Phys. Chem. Chem. Phys., 17, 24173-24181, 10.1039/C5CP04060D, 2015.
- 40 Zhang, J., and Dolg, M.: Global optimization of clusters of rigid molecules using the artificial bee colony
41 algorithm, Phys. Chem. Chem. Phys., 18, 3003-3010, 10.1039/C5CP06313B, 2016.
- 42 Zhang, R., Khalizov, A., Wang, L., Hu, M., and Xu, W.: Nucleation and growth of nanoparticles in the
43 atmosphere, Chem. Rev., 112, 1957-2011, 2012.

- 1 Zhang, R., Wang, G., Guo, S., Zamora, M. L., Ying, Q., Lin, Y., Wang, W., Hu, M., and Wang, Y.:
2 Formation of urban fine particulate matter, *Chem. Rev.*, 115, 3803-3855, 2015.
- 3 Zhang, R., Shen, J., Xie, H. B., Chen, J., and Elm, J.: The role of organic acids in new particle formation
4 from methanesulfonic acid and methylamine, *Atmos. Chem. Phys.*, 22, 2639-2650, 10.5194/acp-
5 22-2639-2022, 2022.
- 6 Zhong, J., Kumar, M., Zhu, C. Q., Francisco, J. S., and Zeng, X. C.: Frontispiece: Surprising Stability of
7 Larger Criegee Intermediates on Aqueous Interfaces, *Angew. Chem. Int. Ed.*, 56, 7740-7744,
8 10.1002/anie.201782761, 2017.
- 9 Zhong, J., Kumar, M., Francisco, J. S., and Zeng, X. C.: Insight into chemistry on cloud/aerosol water
10 surfaces, *Acc. Chem. Res.*, 51, 1229-1237, 2018.
- 11 Zhong, J., Li, H., Kumar, M., Liu, J., Liu, L., Zhang, X., Zeng, X. C., and Francisco, J. S.: Mechanistic
12 Insight into the Reaction of Organic Acids with SO₃ at the Air-Water Interface, *Angew. Chem. Int.*
13 *Ed.*, 131, 8439-8443, 2019.
- 14 Zhong, J., Zhao, Y., Li, L., Li, H., Francisco, J. S., and Zeng, X. C.: Interaction of the NH₂ Radical with
15 the Surface of a Water Droplet, *J. Am. Chem. Soc.*, 137, 12070-12078, 10.1021/jacs.5b07354, 2015.
- 16 Zhong, J., Zhu, C., Li, L., Richmond, G. L., Francisco, J. S., and Zeng, X. C.: Interaction of SO₂ with
17 the Surface of a Water Nanodroplet, *J. Am. Chem. Soc.*, 139, 17168-17174, 2017.
- 18 Zhu, C., Kumar, M., Zhong, J., Li, L., Francisco, J. S., and Zeng, X. C.: New Mechanistic Pathways for
19 Criegee-Water Chemistry at the Air/Water Interface, *J. Am. Chem. Soc.*, 138, 11164-11169,
20 10.1021/jacs.6b04338, 2016.
- 21 Zhu, C., Kais, S., Zeng, X. C., Francisco, J. S., and Gladich, I.: Interfaces select specific stereochemical
22 conformations: the isomerization of glyoxal at the liquid water interface, *J. Am. Chem. Soc.*, 139,
23 27-30, 2017.
- 24 Zhuang, Y., and Pavlish, J. H.: Fate of hazardous air pollutants in oxygen-fired coal combustion with
25 different flue gas recycling, *Environ. Sci. Technol.*, 46, 4657-4665, 2012.

Table 1 The rate constant ($\text{cm}^3 \cdot \text{molecule}^{-1} \cdot \text{s}^{-1}$) for the $\text{SO}_3 + \text{H}_2\text{SO}_4$ reaction and the effective rate constant ($\text{cm}^3 \cdot \text{molecule}^{-1} \cdot \text{s}^{-1}$) for the $\text{SO}_3 + \text{H}_2\text{SO}_4$ reaction with H_2O (100%RH) within the temperature range of 280-320 K

$T/(\text{K})$	280 K	290 K	298 K	300 K	310 K	320 K
k_{DSA}	5.52×10^{-12}	4.60×10^{-12}	3.95×10^{-12}	3.80×10^{-12}	3.13×10^{-12}	2.57×10^{-12}
$k'_{\text{DSA_WM_o}}$	2.12×10^{-13}	2.68×10^{-13}	2.88×10^{-13}	2.89×10^{-13}	2.89×10^{-13}	2.75×10^{-13}
$k'_{\text{DSA_WM_s}}$	1.03×10^{-11}	8.55×10^{-12}	7.42×10^{-12}	7.11×10^{-12}	5.79×10^{-12}	4.60×10^{-12}

k_{DSA} is the rate constant for the $\text{SO}_3 + \text{H}_2\text{SO}_4$ reaction; $k'_{\text{DSA_WM_o}}$ and $k'_{\text{DSA_WM_s}}$ are respectively the effective rate constants for H_2O -assisted $\text{SO}_3 + \text{H}_2\text{SO}_4$ reaction occurring through one-step and stepwise routes.

Table 2 The rate ratio between the $\text{SO}_3 + \text{H}_2\text{SO}_4$ reaction and the hydrolysis of SO_3 at different altitudes in the atmospheres of Earth and Venus

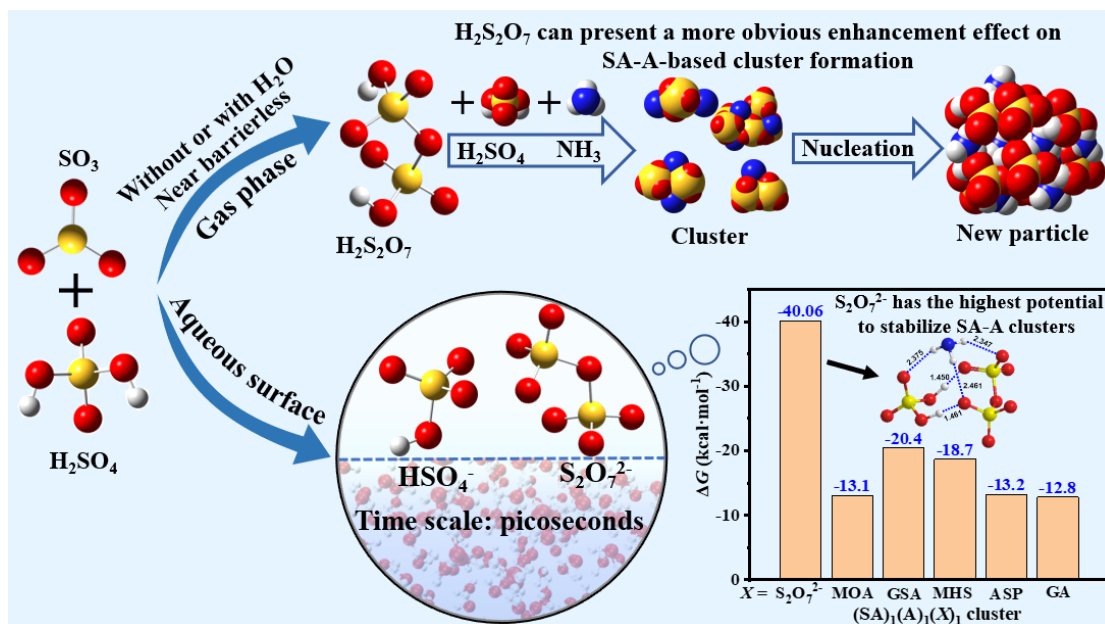
H (km)	T(K)	P (Torr)	$[\text{H}_2\text{O}]^a$	$[\text{H}_2\text{SO}_4]^a$	k_{DSA}	$k_{\text{DSA_WM_s}}$	$k_{\text{SA_WM}}$	$\nu_{\text{DSA}}/\nu_{\text{SA}}$
40	410	2025	1.08×10^{15}	6.15×10^{13}	5.22×10^{-12}	1.43×10^{-12}	2.31×10^{-13}	3.24×10^8
50	340	750	5.17×10^{14}	1.23×10^{14}	1.12×10^{-12}	3.87×10^{-12}	5.43×10^{-13}	3.81×10^{10}
60	320	104	1.72×10^{14}	1.85×10^{14}	1.23×10^{-12}	7.80×10^{-12}	1.37×10^{-12}	5.12×10^{10}
70	270	19	8.61×10^{13}	8.61×10^{13}	1.07×10^{-12}	8.61×10^{-12}	1.82×10^{-12}	5.23×10^{10}

k_{DSA} , $k_{\text{DSA_WM_s}}$ and $k_{\text{SA_SA}}$ are respectively the rate constants for $\text{SO}_3 + \text{H}_2\text{SO}_4$ reaction, H_2O -assisted $\text{SO}_3 + \text{H}_2\text{SO}_4$ reaction occurring through stepwise route and the hydrolysis reaction of $\text{SO}_3 + (\text{H}_2\text{O})_2$.

Table 3 Gibbs free energy (ΔG , kcal·mol⁻¹) for the formation of S₂O₇²⁻···H₂SO₄, S₂O₇²⁻···HNO₃, S₂O₇²⁻···(COOH)₂, H₃O⁺···NH₃, H₃O⁺···H₂SO₄, HSO₄⁻···H₂SO₄, HSO₄⁻···(COOH)₂, HSO₄⁻···HNO₃, H₂SO₄···NH₃, SO₇²⁻···H₂SO₄···NH₃, HOOCCH₂COOH···H₂SO₄···NH₃, HOCCOOSO₃H···H₂SO₄···NH₃, CH₃OSO₃H···H₂SO₄···NH₃ and HOOCCH₂CH(NH₂)COOH···H₂SO₄···NH₃ at 298 K

	S ₂ O ₇ ²⁻ ···H ₂ SO ₄	S ₂ O ₇ ²⁻ ···HNO ₃	S ₂ O ₇ ²⁻ ···(COOH) ₂	H ₃ O ⁺ ···NH ₃	H ₂ SO ₄ ···NH ₃
ΔG	-46.3	-30.6	-39.9	-51.7 (-49.2) ^a	-8.9 (-8.9) ^a
	H ₃ O ⁺ ···H ₂ SO ₄	HSO ₄ ⁻ ···H ₂ SO ₄	HSO ₄ ⁻ ···(COOH) ₂	HSO ₄ ⁻ ···HNO ₃	S ₂ O ₇ ²⁻ ···H ₂ SO ₄ ···NH ₃
ΔG	-27.5 (-27.0) ^a	-41.6	-33.6	-27.8	-40.1
	HOOCCH ₂ COOH ···H ₂ SO ₄ ···NH ₃	HOCCOOSO ₃ H ···H ₂ SO ₄ ···NH ₃	CH ₃ OSO ₃ H ···H ₂ SO ₄ ···NH ₃	HOOCCH ₂ CH(NH ₂)COOH ···H ₂ SO ₄ ···NH ₃	HOCH ₂ COOH ···H ₂ SO ₄ ···NH ₃
ΔG	-13.1 (-13.6) ^b	-20.4 (-22.5) ^c	-18.8 (-20.7) ^d	-13.2 (-14.0) ^e	-12.8 (-13.5) ^f

Energies are given in kcal·mol⁻¹, and calculated at the M06-2X/6-311++G(2df,2pd) theoretical level. References are as follows: [a] Zhong et al., 2019.; [b] Zhang et al., 2018.; [c] Rong et al., 2020.; [d] Gao et al., 2023.; [e] Liu et al., 2021a; [f] Zhang et al., 2017.



Graphic abstract

Figure Caption

Fig. 1 Schematic potential energy surface for the $\text{SO}_3 + \text{H}_2\text{SO}_4 \rightarrow \text{H}_2\text{S}_2\text{O}_7$ reaction; Distances is in angstrom at the M06-2X/6-311++G(2df,2pd) level, while the energy values correspond to the calculations at the CCSD(T)-F12/cc-pVDZ-F12//M06-2X/6-311++G(2df,2pd) level. The pre-reactive complex and TS for the route of DSA formation from the $\text{SO}_3 + \text{H}_2\text{SO}_4$ reaction with H_2O was denoted by “IM_{DSA_WM}” and “TS_{DSA_WM}”, respectively, while the corresponding pre-reactive complex and TS for the process of SA formation from the hydrolysis of SO_3 with H_2SO_4 was respectively labeled as “IM_{SA_SA}” and “TS_{SA_SA}”

Fig. 2 Top panel: Snapshot structures taken from the BOMD simulations, which illustrate H_2O -induced the formation of $\text{S}_2\text{O}_7^{2-} \cdots \text{H}_3\text{O}^+$ ion pair from the reaction of SO_3 with HSO_4^- at the air-water interface. Lower panel: time evolution of key bond distances (S-O1, O2-H1, and O3-H1) involved in the induced mechanism

Fig. 3 Top panel: Snapshot structures taken from the BOMD simulations, which illustrate the hydration reaction mechanism of SO_3 mediated by HSO_4^- at the air water interface. Lower panel: time evolution of key bond distances (S-O1, O1-H2, O5-H2, O2-H1, O3-H4 and O4-H3) involved in the hydration mechanism

Fig. 4 Top panel: Snapshot structures taken from the BOMD simulations, which illustrate the deprotonation of $\text{H}_2\text{S}_2\text{O}_7$ at the air water interface. Lower panel: time evolution of key bond distances (O1-H1, O1-H2, O3-H2 and H2-O4) involved in the hydration mechanism

Fig. 5 The Gibbs free energy ($\text{kcal}\cdot\text{mol}^{-1}$) diagram of $(\text{DSA})_x(\text{SA})_y(\text{A})_z$ ($z \leq x + y \leq 3$) clusters at 278.15K and 1 atm. “A” refers to sulfuric acid, “D” refers to disulfuric acid and “N” refers to ammonia

Fig. 6 Cluster formation rates J ($\text{cm}^{-3} \text{ s}^{-1}$) against the of DSA monomer concentration (unit: $\text{molecules}\cdot\text{cm}^{-3}$) under different temperatures (218.15, 238.15, 258.15, 278.15 and 298.15 K) where $[\text{SA}] = 10^7 \text{ molecules}\cdot\text{cm}^{-3}$ and $[\text{A}] = 10^9 \text{ molecules}\cdot\text{cm}^{-3}$

Fig. 7 Simulated cluster formation rates J ($\text{cm}^{-3} \text{ s}^{-1}$) as a function of (a) $[\text{SA}]$, (b) $[\text{A}]$, with different concentrations of disulfuric acid $[\text{DSA}]$ of 10^4 (red), 10^5 (blue), 10^6 (green), 10^7 (purple) and 0 $\text{molecules}\cdot\text{cm}^{-3}$ (black, pure-SA-A), at $T = 238.15 \text{ K}$

Fig. 8 (a) The main pathways of clusters growing out of the research system under the conditions where 218.15 K, 238.15K and 258.15 K, $[\text{SA}] = 10^8 \text{ molecules}\cdot\text{cm}^{-3}$, $[\text{A}] = 10^9 \text{ molecules}\cdot\text{cm}^{-3}$, and $[\text{DSA}] = 10^6 \text{ molecules}\cdot\text{cm}^{-3}$; (b) The contribution of different concentrations of DSA to the main cluster formation pathway at 218.15 K, 238.15 K and 258.15 K is shown in the pie charts

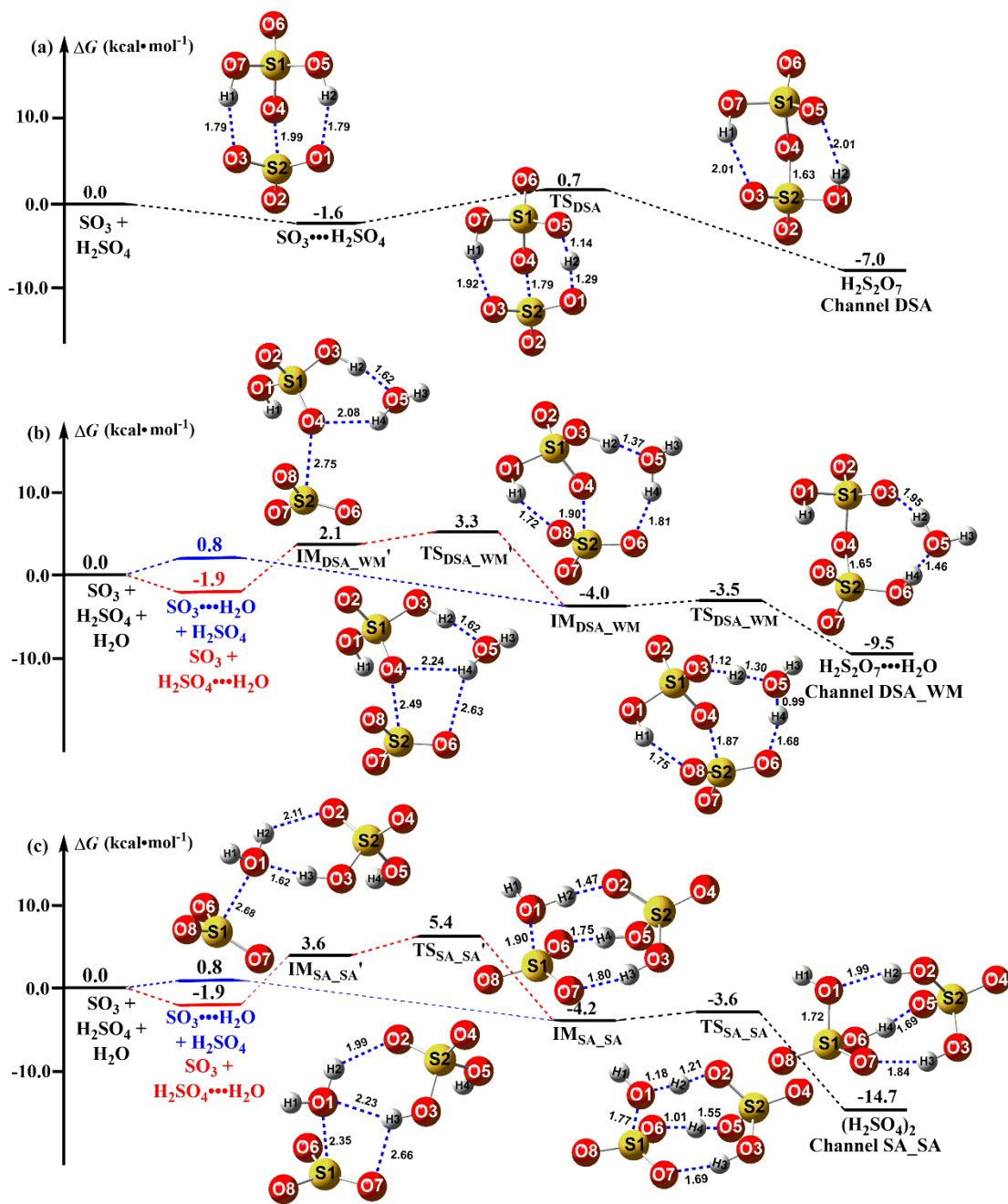


Fig. 1

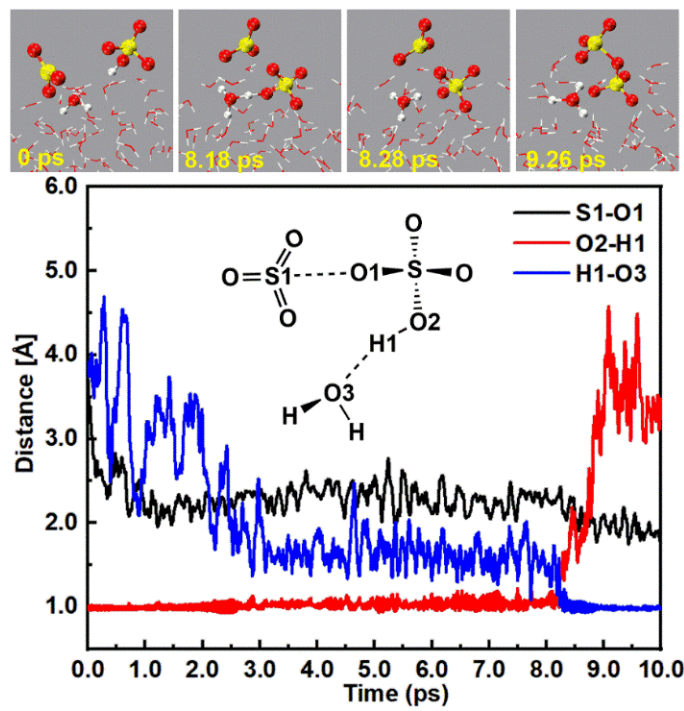


Fig. 2

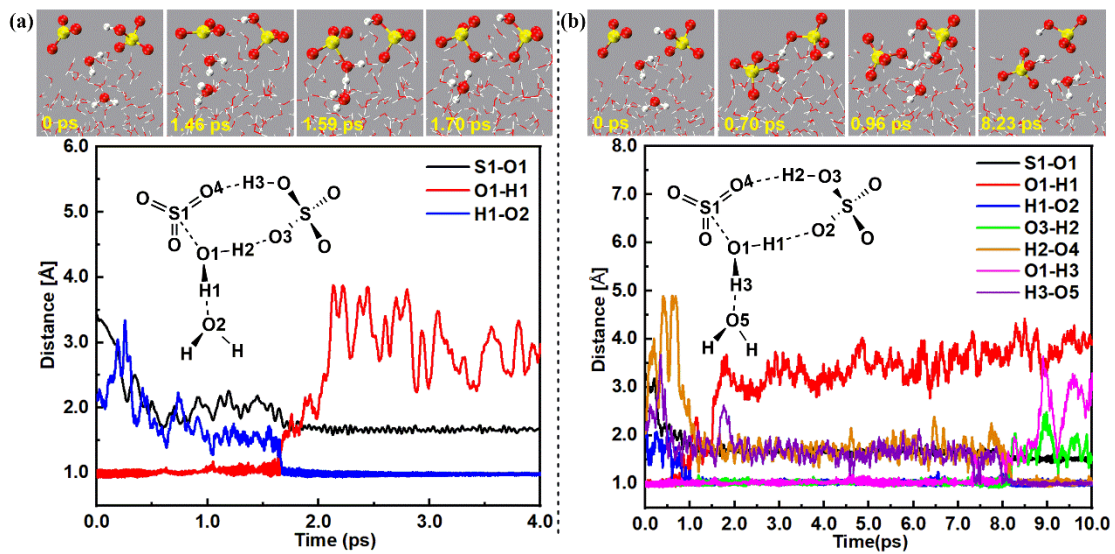


Fig. 3

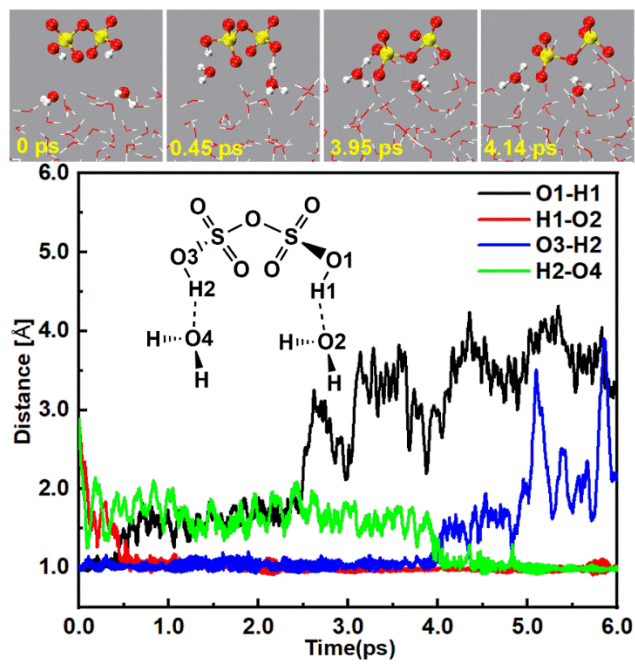


Fig. 4

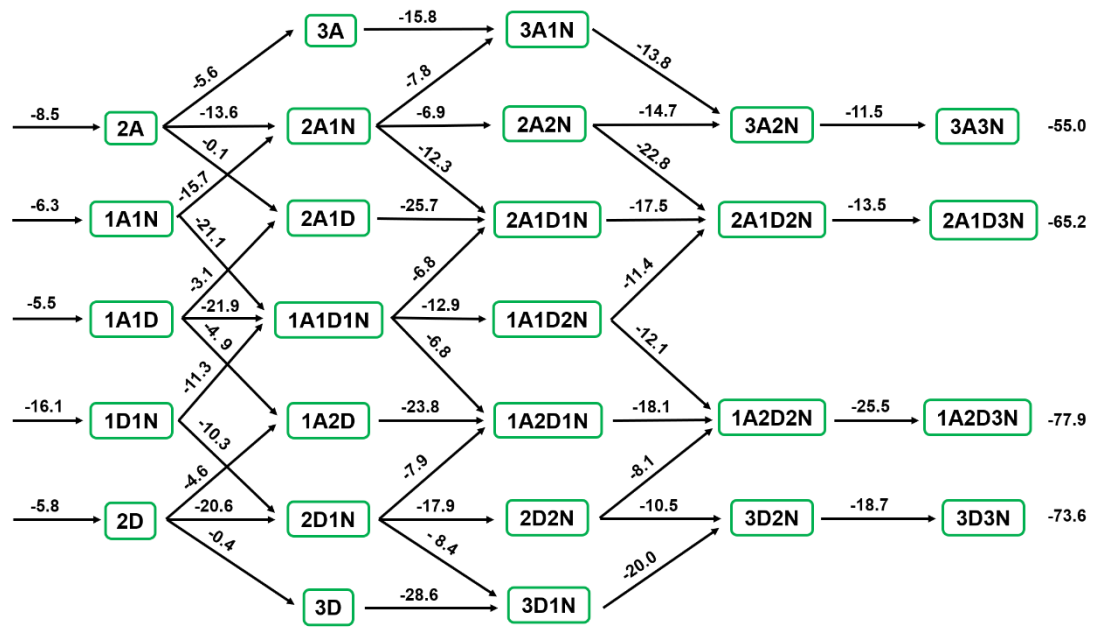


Fig. 5

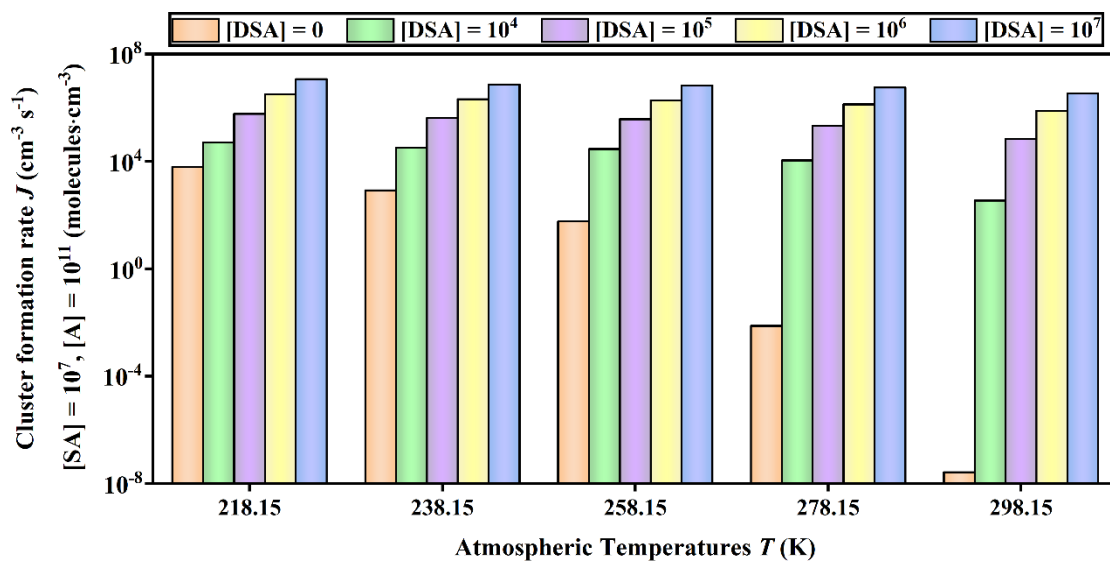


Fig. 6

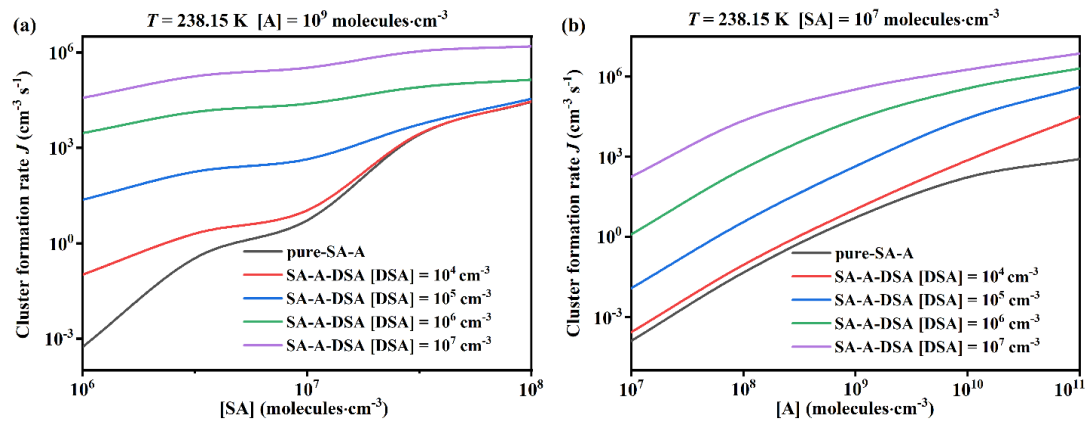


Fig. 7

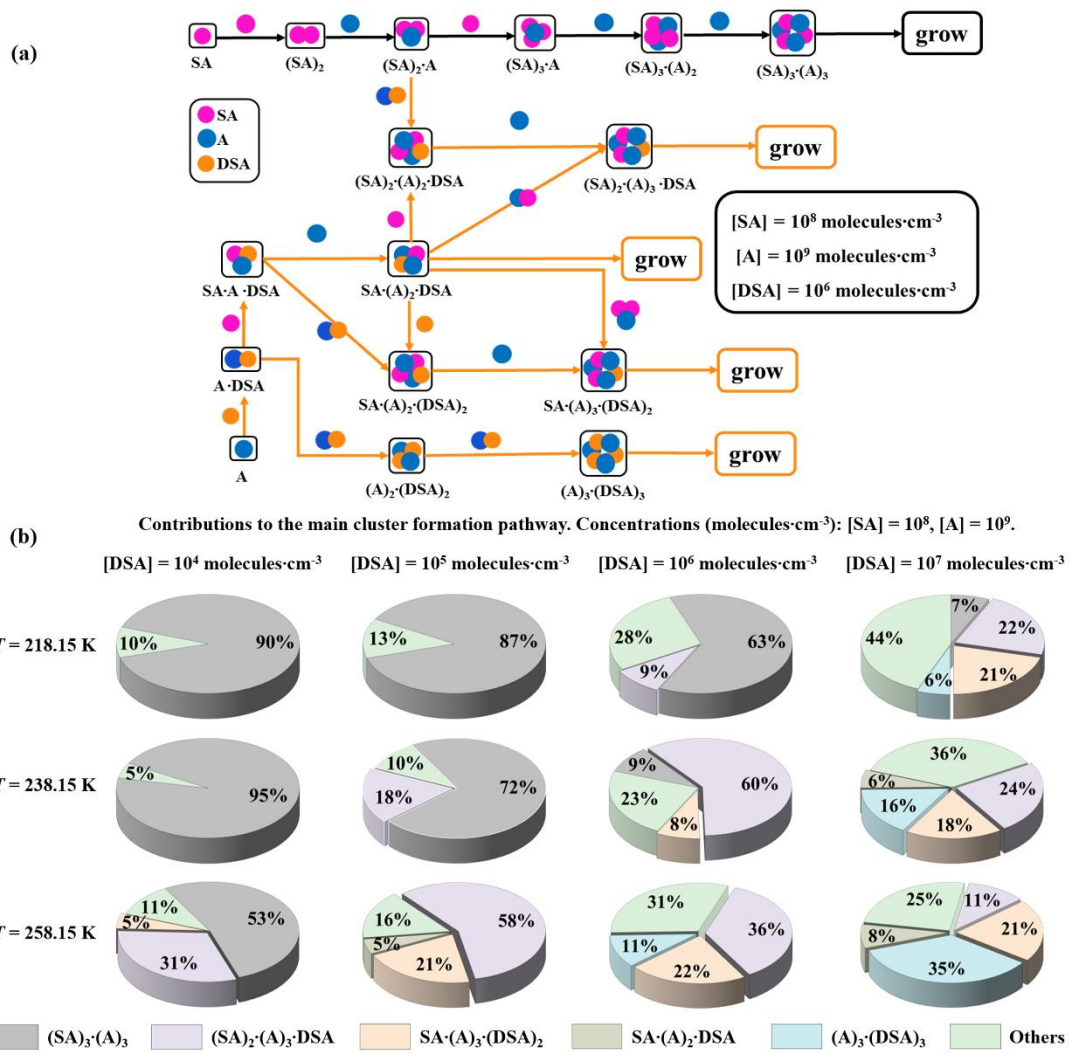


Fig. 8